


Review

Molecular Gas Kinematics in Local Early-Type Galaxies with ALMA

Ilaria Ruffa ^{1,2,*}  and Timothy A. Davis ^{1,*}

¹ Cardiff Hub for Astrophysics Research & Technology, School of Physics & Astronomy, Cardiff University, Queens Buildings, The Parade, Cardiff CF24 3AA, UK

² INAF—Istituto di Radioastronomia, Via P. Gobetti 101, 40129 Bologna, Italy

* Correspondence: ruffai@cardiff.ac.uk (I.R.); davist@cardiff.ac.uk (T.A.D.)

Abstract: Local early-type galaxies (ETGs) are mostly populated by old stars, with little or no recent star formation activity. For this reason, they have historically been believed to be essentially devoid of cold gas, which is the fuel for the formation of new stars. Over the past two decades, however, increasingly-sensitive instrumentation observing the sky at (sub-)millimetre wavelengths has revealed the presence of significant amounts of cold molecular gas in the hearts of nearby ETGs. The unprecedented capabilities offered by the Atacama Large Millimeter/submillimeter Array (ALMA), in particular, have allowed us to obtain snapshots of the central regions of these ETGs with unprecedented detail, mapping this gas with higher sensitivity and resolution than ever before possible. Studies of the kinematics of the observed cold gas reservoirs are crucial for galaxy formation and evolution theories, providing, e.g., constraints on the fundamental properties and fuelling/feedback processes of super-massive black holes (SMBHs) at the centre of these galaxies. In this brief review, we summarise what the first 10 years of ALMA observations have taught us about the distribution and kinematics of the cold molecular gas component in nearby ellipticals and lenticulars.

Keywords: galaxies: ellipticals and lenticulars; ISM: molecular gas; ISM: kinematics



Citation: Ruffa, I.; Davis, T.A.

Molecular Gas Kinematics in Local
Early-Type Galaxies with ALMA.

Galaxies **2024**, *12*, 36.

[https://doi.org/10.3390/](https://doi.org/10.3390/galaxies12040036)

[galaxies12040036](https://doi.org/10.3390/galaxies12040036)

Academic Editor: Alexei V. Moiseev

Received: 15 May 2024

Revised: 24 June 2024

Accepted: 27 June 2024

Published: 2 July 2024



Copyright: © 2024 by the authors. Licensee MDPI, Basel, Switzerland. This article is an open access article distributed under the terms and conditions of the Creative Commons Attribution (CC BY) license (<https://creativecommons.org/licenses/by/4.0/>).

1. Introduction

High-quality imaging and spectroscopic surveys carried out over the past two decades (such as the Sloan Digital Sky Survey, SDSS; [1]) have revealed the existence of a clear bi-modality in the colour and mass distribution of galaxies in the local Universe (i.e., within $z < 0.1$; e.g., [2]). One mode consists of late Hubble-type (disc) galaxies characterised by significant ongoing star formation (and thus blue optical colours), stellar masses $M_* \lesssim 10^{10.5} M_\odot$, and a tight correlation between their star formation (SF) rate and M_* (known as the “star-forming main sequence”; e.g., [3]). The other population consists of the so-called early-type galaxies (ETGs) made up of both ellipticals and lenticulars. These are generally dominated by old stars, which likely formed in bursts at the time of their high-redshift progenitors, the so-called dusty star-forming galaxies (DSFG; also known as sub-millimetre galaxies, SMGs; see, e.g., [4–6]). There is very little or no ongoing SF in modern-day ETGs, and they have typical masses of $M_* \gtrsim 10^{10.5} M_\odot$. Therefore, in classic optical colour-magnitude diagrams, ETGs give rise to what has been dubbed the “red- or passive-sequence” (e.g., [7]).

It is now widely believed that this bi-modality is a result of galaxy evolution (e.g., [8]). In this scenario, the transition of galaxies from star-forming discs into “red and dead” spheroids is driven by the availability within the inter-stellar medium (ISM) of cold gas (i.e., the fuel for star formation), which is in turn regulated by the balance between gas accretion and depletion processes (e.g., [9]). This transition occurs relatively quickly (as only a very minor fraction of galaxies populates the region between the two sequences, the so-called “green valley”) and –once completed– it is permanent (at least in the majority of cases).

Galaxy formation and evolution theories still struggle to reproduce the observed properties of red sequence galaxies: how they are kept as passive spheroids while growing in mass up to $M_* \sim 10^{12} M_\odot$ and how the fuelling/feedback processes of their central super-massive black holes (SMBHs) are powered and sustained are only some subjects of long-standing debates (e.g., [10–12]).

Due to the optical properties described above, local ETGs have historically been believed to be essentially devoid of cold gas. Over the past 20 years, however, increasingly-sensitive millimetre-wave instruments (such as the Institut de Radioastronomie Millimétrique 30 m single-dish, IRAM-30m; the Northern Extended Millimetre Array, NOEMA; and the Combined Array for Research in Millimeter-wave Astronomy, CARMA) have revealed that molecular gas is present in at least $\approx 25\%$ of local ETGs [13–22], and this detection rate is insensitive to galaxy mass (but potentially not to the dynamical state of the system; [19,22]). Over the past decade in particular, the resolution and sensitivity provided by the Atacama Large Millimeter/submillimeter Array (ALMA) has allowed us to obtain snapshots of their cores with unprecedented detail and to accurately map the distribution and kinematics of this gas, thus opening entirely new avenues in the study of cold ISM in this type of object (see, e.g., [23–54] and references therein).

The observation of significant amounts of cold gas in red sequence galaxies triggered the idea that these objects also experience cyclical regeneration of their gaseous reservoirs, which must then be retained for a while within their deep potential wells. How the bulk of the cold gas in local ETGs re-forms and settles down, however, is still an open question. It may be either internally re-generated (through, e.g., hot halo cooling) or externally accreted (through interactions or minor mergers). Evidence is mounting that the large-scale environment where the galaxy is located plays a crucial role in determining the preferred mechanism. In this scenario, ETGs located in high-density environments (i.e., at the centre of rich groups and clusters) may preferentially re-form the bulk of their cold gas reservoirs via cooling of their hot atmospheres. External accretion (mainly in the form of interaction with neighbouring galaxies) may instead represent the dominant cold gas replenishing mechanism for ETGs in poorer environments (e.g., isolated or poor groups). In either case, an additional contribution may come from the mass returned to the ISM by evolved (primarily asymptotic giant branch) stars (up to $\sim 30\%$ of the stellar mass initially formed, depending on the initial mass function and age (e.g., [55])). The many details of these processes, however, are still hotly debated (see, e.g., [22,33,34,41,44,49,56] for extensive discussions in this regard).

Independently of their large-scale environment, massive spheroids are also the preferential hosts of jetted active galactic nuclei (AGN), which are those producing (relatively) strong kinetic feedback in the form of collimated, relativistic outflows of non-thermal plasma (i.e., the radio jets; (see, e.g., [57])). This AGN category currently includes all types of radio galaxies (RGs), the most powerful low-ionization nuclear emission-line regions (LINERs), and some quasars/Seyferts (e.g., [58,59]). The first decade of ALMA observations have enabled detailed studies of the cold gas reservoirs in each of these jetted AGN types, helping to improve our understanding of their powering mechanism(s), as well as the complex interplay between radio jets and the surrounding gaseous medium at all spatial scales (from the inner sub-kpc to tens of kpc; e.g., [32,41,44,48,60–64]). In this context, a particularly interesting example is that of low-excitation radio galaxies (LERGs), which are the most common type of RGs at $z < 0.1$. LERGs are typically hosted by the most massive ETGs (with $M_* > 10^{11} M_\odot$; [65]), whereby the central SMBH accretes gas at very low rates ($\ll 1\%$ of the Eddington limit) and produces almost exclusively kinetic feedback (e.g., [33,34,58,65]). Due to their host-galaxy properties, the SMBHs in LERGs have traditionally been believed to be fuelled by direct inefficient accretion of hot X-ray emitting gas from the circumgalactic and/or intergalactic medium (CGM and IGM, respectively; see, e.g., [66]). The detection of large masses of cold gas at their centres, however, started to question this picture, providing new fundamental constraints on the powering mechanism of LERGs (see, e.g., [33,34,41,46]).

In this manuscript, we present a short review of what we have learned in the past 10 years by studying the distribution and kinematics of the molecular gas in local ETGs when observing them at very high resolution and sensitivity with ALMA.

2. Molecular Gas in Early-Type Galaxies

Carbon monoxide (CO) is the most used molecular gas tracer. It is the most abundant molecule after H₂ (which is rather difficult to detect in emission; see, e.g., [67,68]) and has low requirements in terms of both excitation temperature (i.e., $T_{\text{ex}} = 5.53$ K for the ground $J = 1 \rightarrow 0$ rotational transition) and critical density (n_{crit} ; i.e., the density at which collisional excitation balances spontaneous radiative de-excitation, which, for CO, is $\gtrsim 2200$ cm⁻³). All this makes CO relatively easy to detect in extragalactic sources (e.g., [69]). Other molecules, such as formylion (HCO⁺), carbon monosulfide (CS), and hydrogen cyanide (HCN), are instead the most used tracers for the dense ($n_{\text{crit}} > 10^4$ cm⁻³) molecular gas component (e.g., [42,70,71]). The rotational transitions of all these lines up to $J_{\text{upper}} = 8$ –10 (up to $J_{\text{upper}} = 19$ for CS) have rest frequencies between ≈ 100 GHz and ≈ 900 GHz, making them ideal for ALMA observations in nearby galaxies. An inexhaustive search of the ALMA Science Archive carried out at the time of writing finds available observations of different CO lines (mostly of the transitions with $J_{\text{upper}} = 1, 2$ or 3) and/or dense molecular gas tracers for about 150 single ETGs within $z \lesssim 0.05$. Of these, about 90 have been published so far, and about 70 were clearly detected (at least) in CO. In the following, we summarise the main properties in terms of gas distribution and kinematics that have been inferred from these studies. We note that, for clarity, in this review we divide the ETG population into three different classes: normal ETGs (standard, passive spheroids without any clear signs of nuclear activity), jetted AGN hosts, and brightest central galaxies (BCGs; i.e., very massive ETGs at the centre of rich groups and clusters, typically also hosting a jetted AGN). We also note that the normal ETGs and non-BCG jetted AGN hosts discussed in the following lie in a variety of large-scale environments (isolated, in a pair, in poor groups, or towards the outskirts of massive clusters).

2.1. Cold Gas Content and Distribution

Advances in millimetre instrumentation mean that we are now able to detect and map the gas reservoirs in ETGs, even in systems with low gas masses. The typical molecular gas masses found in ETGs studied to date range from $\sim 10^7$ to $\sim 10^8$ M_⊙ but can even go up to $\sim 10^9$ – 10^{10} M_⊙ in some exceptional cases (see, e.g., [23,33,38,72,73]). We caution, however, that these masses can have relatively large uncertainties, mainly introduced by the adopted CO-to-H₂ conversion factor (see [67] for a comprehensive review of this subject) and the ratio over the ground CO transition (when using higher- J CO lines for the estimation; see, e.g., [33,41] for discussions in this regard).

In normal ETGs and jetted AGN hosts (including a few BCGs), the detected CO emission is usually observed to be distributed in thin disc-like structures, extending on scales from a few hundred parsecs to a few kpc around the nuclear regions of the host galaxy (see Figure 1). Such compact molecular gas morphologies are also very smooth (even when observed at spatial resolutions as high as 10 pc) and have typical mean surface densities in the range 10^2 – 10^3 M_⊙ pc⁻² (see, e.g., [74]). Altogether, these characteristics have been interpreted as an indication of gas that has mostly settled into the potential well of the host galaxy.

Nuclear gas deficiencies or proper central holes (i.e., ring-like shapes) are also observed in about 20% of the cases, including both normal ETGs and jetted AGN hosts (in roughly equal fractions; e.g., [21,29,33,38,75–77]) (see Figure 2). The size of such circumnuclear cavities usually ranges from a few tens to a few hundreds of parsecs, and their origin is still puzzling. Some mechanism may either dissociate the molecular gas or prevent it from forming (or accumulating) in the very centre of the galaxy. This can occur in the presence of an intense radiation field, such as the one due to strong X-ray radiation from a radiatively efficient (quasar-like) AGN (producing the so-called X-ray dissociation

regions, XDRs). Various studies suggest that XDRs are particularly effective in dissociating molecules such as HCO^+ (see, e.g., [78,79]). On the other hand, in radiatively-inefficient (LINER-like) AGN, the X-ray radiation arising from the accretion process is much less extreme in terms of dissociating power. Therefore, in cases like these, the molecular gas at the centre can simply be much denser and excited towards high- J transitions due to X-ray heating or shocks and compression induced by an interaction with the expanding radio jets (see Section 2.2 for details). When this occurs, the central gap is usually filled when observing CO lines with $J_{\text{upper}} \geq 3$ and/or dense molecular gas tracers (e.g., [79]). Prominent molecular gas outflows (due to either jet-induced or radiative AGN feedback) have been also indicated as particularly plausible processes for the removal of gas from the circumnuclear regions (e.g., [60,80]; see also [81] for a recent review of the effects of AGN feedback on the circumnuclear gas reservoirs).

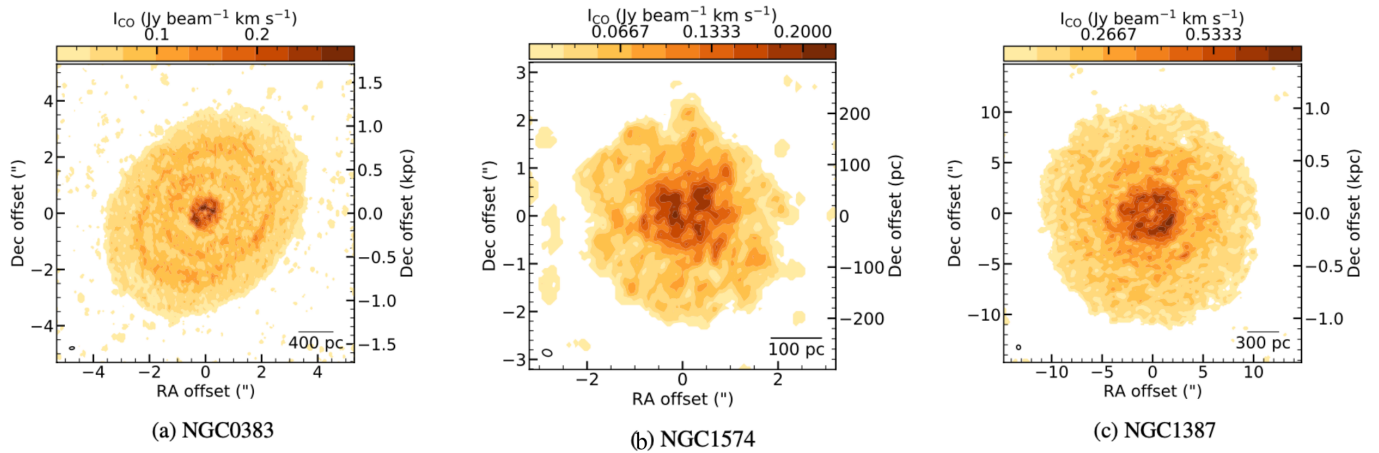


Figure 1. Integrated intensity (i.e., moment 0) maps of the CO(2-1) transition observed at high-resolution with ALMA in three local ETGs (as labelled at the bottom of each panel). These are taken as an example of normal ETGs and (non-BCG) jetted AGN hosts that are characterised by compact and smooth disc-like molecular gas structures extending around the central galaxy regions (see the text for details). The synthesised beam and scale bar are shown in the bottom left and bottom right corners, respectively, of each panel. The physical resolution reached is similar in each case (≈ 30 pc). The bar on top of each panel shows the colour scale in $\text{Jy beam}^{-1} \text{ km s}^{-1}$, and coordinates are given relative to the image phase centre. The maps are reproduced from Davis et al. [74].

Dynamical effects can also affect the distribution and survival of molecular gas in those areas, thus favouring the formation of nuclear cavities. For instance, the strong shear or tidal acceleration expected near the SMBH can disrupt gas clouds. Non-axisymmetric gravitational instabilities induced by stellar bars can also give rise to nuclear gaps, relying on bar-induced gravitational torques that force the gas outwards to the inner Lindblad resonance (ILR), or inwards on to the central SMBH (e.g., [82]). Stellar bars, however, also give rise to characteristic features in molecular gas velocity curves (i.e., position-velocity diagrams, PVDs), especially in galaxies with high inclination angles with respect to the line of sight (i.e., $\theta_{\text{inc}} \gtrsim 60^\circ$). In these cases, molecular gas PVDs typically show X shapes or sharp edges near the turnover radius (i.e., the radius that marks the transition between the central rising and the external flat part of the velocity curve; see Section 2.2). These are both clear signatures indicative of the presence of two velocity components along the line of sight: an inner rapidly rising component associated with gas located within the ILR, and an outer slowly rising component associated with gas on nearly circular orbits beyond co-rotation (e.g., [21,73,83]). Based on all the above, it is clear that high-quality, multi-wavelength observations of the various galaxy components (e.g., stars, radio jet, etc.), in conjunction with those of multiple molecular gas transitions, are the key to discriminating between different mechanisms and to drawing solid conclusions about the origin of the observed circumnuclear molecular gas holes.

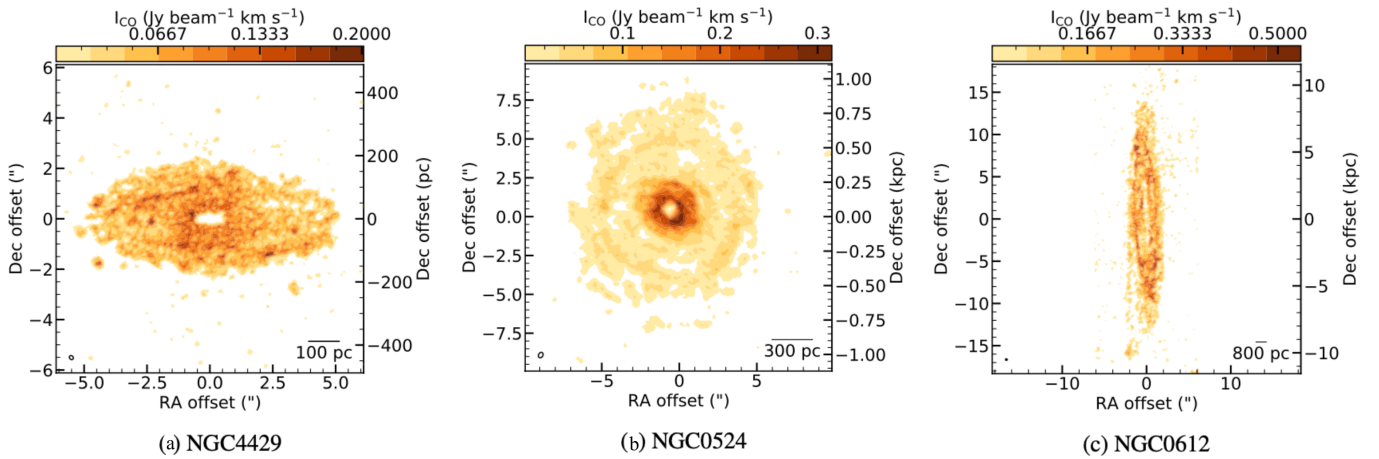


Figure 2. Integrated intensity (i.e., moment 0) maps of the CO(2-1) transition observed at high-resolution with ALMA in three local ETGs (as labelled at the bottom of each panel). These are taken as an example of normal ETGs and (non-BCG) jetted AGN hosts, which are characterised by evident nuclear gas deficiencies or proper ring-like shapes. The synthesised beam and scale bar are shown in the bottom left and bottom right corners, respectively, of each panel. The physical resolution reached is similar in each case (≈ 30 pc). The bar on top of each panel shows the colour scale in $\text{Jy beam}^{-1} \text{ km s}^{-1}$, and coordinates are given relative to the image phase centre. The maps are reproduced from Davis et al. [74].

The distribution of molecular gas in BCGs is often different from that described above, with large amounts of cold gas typically detected in the form of kpc-scale filamentary or blob-like structures (e.g., [32,36,37,44,61,84–88]). As already mentioned in Section 1, these are thought to be cooling from the hot, X-ray-emitting intra-cluster (or intra-group) medium, as described, for instance, in the framework of chaotic cold accretion (CCA) models (see, e.g., [89–92]). According to CCA models, thermal instabilities in the hot halo lead to the formation of decoupled dense gas structures, being distributed into clouds and filaments while cooling down to $T \ll 10^3$ K. Stochastic dissipative collisions between such cold gas structures then significantly reduce their angular momentum, causing them to chaotically “rain” towards the central SMBH. Recent works demonstrate that relatively tight correlations exist between the molecular gas mass and the hot halo properties (i.e., temperature, mass, and luminosity) of group-/cluster-centered ETGs [93], providing further evidence of a close hot-cold gas connection in these objects. A notable case among this category is that of NGC 5044, a well-known ETG at the centre of an X-ray bright group observed multiple times with ALMA in CO(2–1) [84,86] (Figure 3). These data reveal the presence of 17 cold gas clouds within the central ~ 6 kpc of the galaxy, each extending on scales of less than 300 pc. Interestingly, these clouds appear to be mostly co-spatial with the warm gas phase (as visible in the $\text{H}\alpha + [\text{N II}]$ map shown in the left panel of Figure 3) and with X-ray emission [85], resulting in the multi-phase cooling gas distribution predicted in CCA simulations [92].

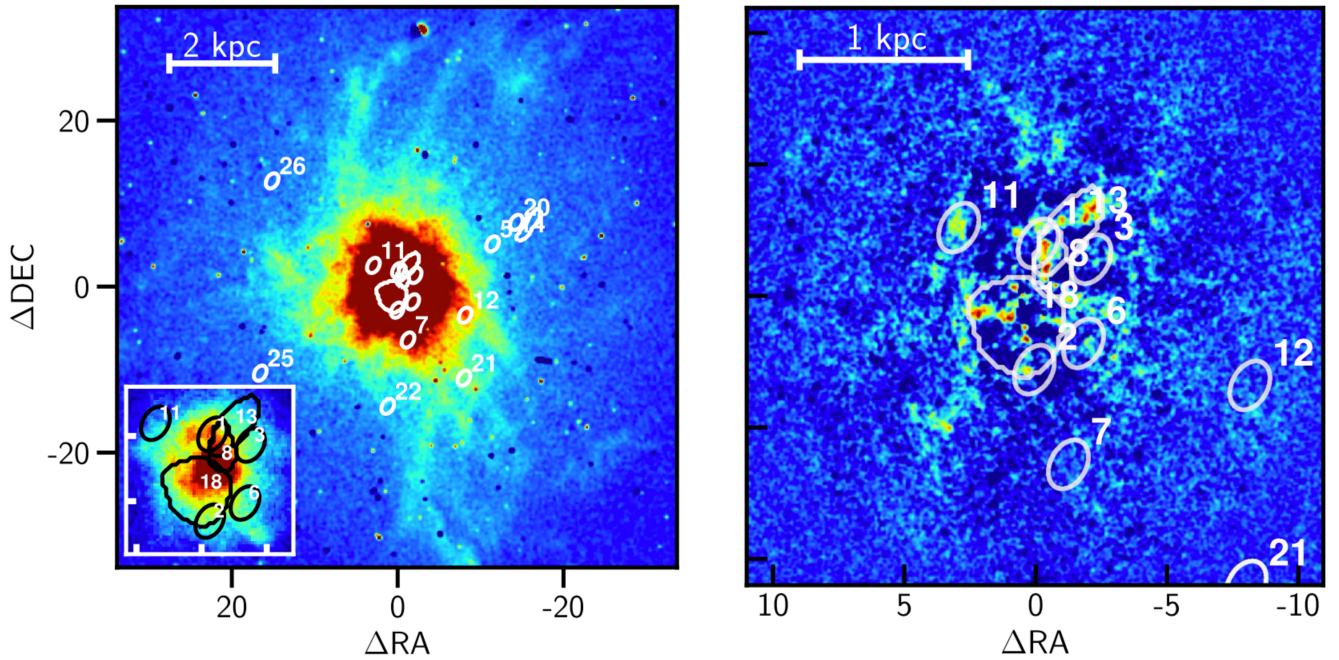


Figure 3. Optical $H\alpha+[NII]$ integrated intensity map (**left panel**) and dust absorption map (**right panel**) of the BCG NGC 5044 overlaid in black (in the zoomed-in inset on the **left panel**) and white with the contours of the 17 CO(2-1) clouds detected with ALMA. The colour sequence (going from blue to red) indicates increasing values of ionized gas intensities and dust absorption. The maps are reproduced with permission from Temi et al. [86]. See the text for details.

2.2. Molecular Gas Kinematics

Quantitative details on the dynamical state of the molecular gas in ETGs are typically obtained from the 3D kinematic modelling of spatially-resolved gas distributions (using publicly-available tools such as the Kinematic Molecular Simulation tool, KINMS [75] and ^{3D}BAROLO [94]) and/or from the harmonic decomposition of 2D line-of-sight gas velocity maps (using packages such as KINEMETRY [95]). Qualitatively, information on the gas kinematics can be also inferred by eye from the integrated line profiles and the classic 3D imaging data products, such as the mean line-of-sight velocity map (moment 1) and the PVDs. In the following, we briefly summarise the results obtained from these types of analyses, splitting the discussion of normal ETGs and jetted AGN hosts (including BCGs). We note that maps of the mean line-of-sight velocity dispersion (moment 2) are also typically used to obtain spatial information on the line velocity broadening and thus on the corresponding gas dynamical state. We caution, however, that moment maps of order higher than 1 are the most severely affected by the signal-to-noise ratio (S/N) and spatial resolution of the line detection (due to the way they are defined; see, e.g., <https://spectral-cube.readthedocs.io/en/latest/moments.html#linewidth-maps>, accessed on 20 June 2024), becoming essentially meaningless when the S/N is too low (e.g., $\lesssim 5$) and/or the detected gas distribution is unresolved or barely resolved. Furthermore, even in cases where the gas distribution is well-resolved, line-of-sight velocity dispersions can be significantly inflated due to observational effects. Among these, beam smearing (i.e., contamination from partially resolved or unresolved velocity gradients within the host galaxy) usually dominates in regions of large velocity gradients, such as the inner regions of galaxies. For this reason, it is highly recommended to always validate the observed velocity dispersion (σ_{gas}) of resolved gas distributions by means of a full 3D kinematic modelling that takes into account these sorts of observational effects (and thus provides an estimate of the intrinsic σ_{gas} ; see, e.g., [25,46]). The values of σ_{gas} discussed in the following can all be considered intrinsic.

2.2.1. Normal ETGs

Studies of molecular gas kinematics (mostly based on ALMA observations of the CO(2-1) transition) show that, in normal ETGs, the gas is regularly rotating. Any departure from symmetry (such as inclination or velocity warps) and secondary kinematic components (such as inflow/outflow motions) are negligible or completely absent in the majority of these cases (e.g., [25,26,29,52,70,96–98]). For instance, by analysing the dynamical state of the molecular gas in five local normal ETGs observed at high resolution (≤ 100 pc) in CO(2-1) with ALMA, Boizelle et al. [26] found that, in all the targets, deviations from models assuming gas in pure circular motions were very small ($\lesssim 10$ km s $^{-1}$) and disc warpings of low magnitude ($\lesssim 10^\circ$). This is also consistent with earlier results from the ATLAS 3D survey [99], which were obtained by studying the molecular gas kinematics of ≈ 30 normal (gas-rich) ETGs observed in CO(1-0) with CARMA (see [21,75]). These findings have been generally interpreted as an indication of gas that is both dynamically and morphologically relaxed and thus fully settled into the potential well of the host galaxy. In cases like these, the mean line-of-sight velocity maps and integrated line profiles respectively show fairly regular/smooth velocity gradients and prominent, nearly-symmetric double-horned shapes characteristic of rotating bodies (see Figure 4, left and middle panels, respectively). The PVDs extracted along the major axis of such regularly-rotating gas distributions are usually characterised by a steep velocity gradient at the centre, followed by a velocity flattening on larger scales (see Figure 4, right panel). These PVDs also do not present any clear asymmetry and/or secondary kinematic component (with the exception, in well-resolved cases such as the one shown in Figure 4, of the Keplerian upturn at the very centre of the gas distribution; see Section 3 for details). In these cases, the typical mean gas velocity dispersion is in the range $\sigma_{\text{gas}} \sim 10\text{--}20$ km s $^{-1}$ (where these are values found by averaging throughout the disc/ring (see, e.g., [34,46,73,100])). As a consequence, the molecular gas in normal ETGs is consistent with being dynamically cold, and the disc/ring is fully rotationally supported (with typical $v_{\text{rot}}/\sigma_{\text{gas}}$ ratios ≥ 10 , where v_{rot} is the de-projected circular velocity of the gas at the turnover radius (see, e.g., [101])).

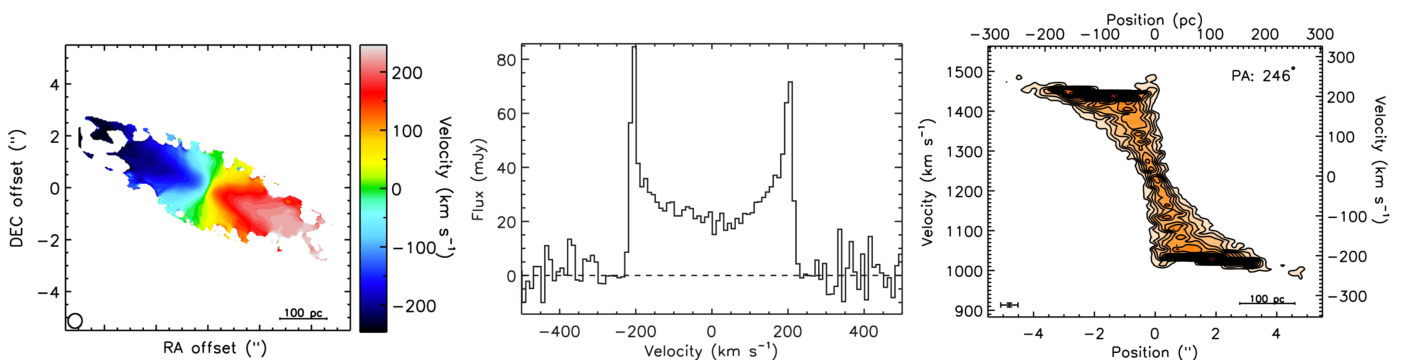


Figure 4. CO(2-1) mean line-of-sight velocity (moment 1) map (**left panel**), integrated spectral profile (**middle panel**), and major axis position-velocity diagram (PVD; **right panel**) of the normal ETG NGC 4697. All maps are reproduced with permission from Davis et al. [25]. In the left panel, the synthesised beam is shown in the bottom left corner, and the colour bar to the right shows the colour scale in km s $^{-1}$. A scale bar is also shown in the bottom right corner of the left and right panels. Coordinates are given as offsets (in arcseconds) relative to the image phase centre.

2.2.2. Jetted AGN Hosts and Jet–ISM Interactions

Fully relaxed CO discs/rings are not a standard feature of all local ETGs. Indeed, a number of works have now demonstrated that clear differences can be observed in the molecular gas kinematics of jetted AGN hosts (e.g., [34,46,48,60,62,102,103]). For instance, Ruffa et al. [34,41,46] carried out the 3D kinematic modelling of the CO(2-1) transition in seven nearby ETGs hosting LERGs. In all cases, they found that—while the bulk of the gas can be still considered as regularly rotating and dynamically cold—localised distortions

in both the morphology and kinematics can be ubiquitously observed. These cannot be reproduced by simple axisymmetric models assuming gas in pure circular motions, thus indicating the presence of unrelaxed gas substructures (a small compilation of these examples is presented in Figure 5). In particular, multiple kinematic components and/or warps (i.e., tilted or s-shaped velocity iso-contours) can be identified in almost all cases, the former with velocities up to $\approx 600 \text{ km s}^{-1}$ (see, e.g., the lower panel of Figure 5), and the latter with magnitudes $\gtrsim 40^\circ$ (see, e.g., the upper left panel of Figure 5). Similar features can arise from a number of different physical processes, such as stellar bars, settling mechanisms, and inner spiral perturbations, without necessarily invoking AGN feedback (see, e.g., [34,46] for comprehensive discussions in this regard). However, the fact that such disturbances are systematically observed in ETGs hosting AGN with active radio jets (as opposed to that found in their inactive counterpart; see above) suggests that there might be a correlation between the two (see, e.g., [63]). A detailed discussion of the role of radio jets in modifying the physics and kinematics of the molecular gas on the (sub-)kpc scales of nearby active galaxies is beyond the scope of this work. However, in the following, we briefly review the notions and findings that are most relevant in this framework.

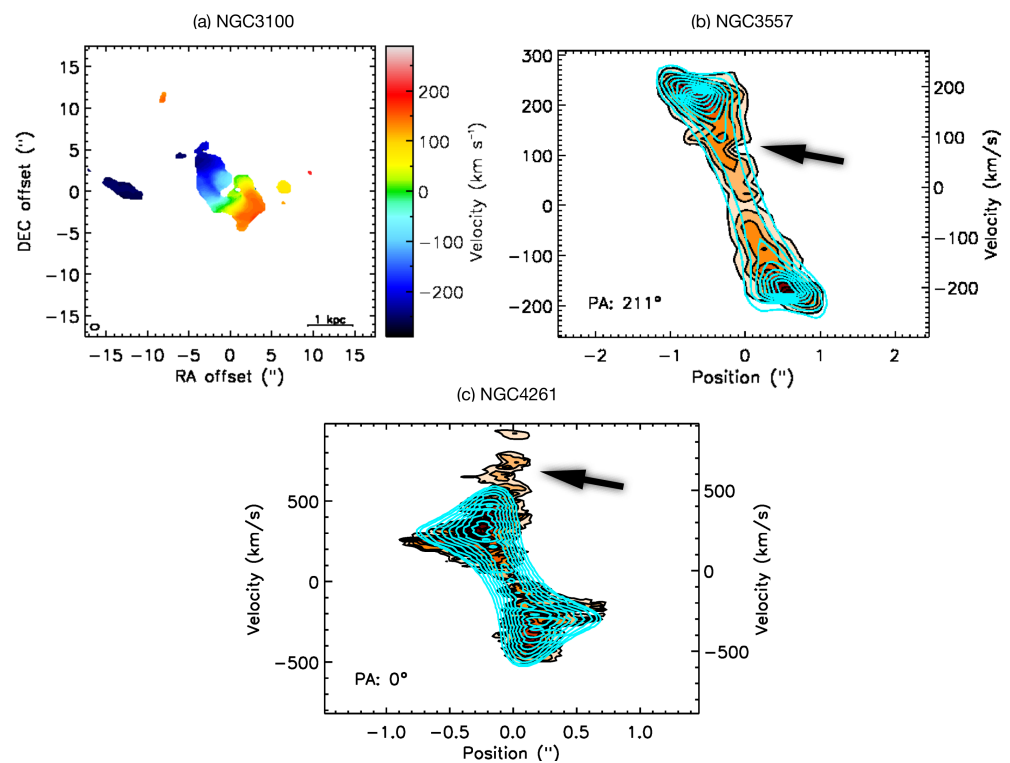


Figure 5. CO(2-1) mean line-of-sight velocity (moment 1) map of NGC3100 (**top-left panel**) and major axis PVDs of NGC3557 and NGC4261 (**top-right and bottom panels**, respectively), all taken as examples of jetted AGN hosts and reproduced from Ruffa et al. [34,46]. In the **top right** and **bottom panels**, the contours of the best-fitting kinematic model assuming gas in pure circular motions are overlaid in cyan, clearly highlighting the presence of unrelaxed gas substructures that are not reproduced by such a simple axisymmetric model (see Ruffa et al. [34,46] for details). The black arrows point to the location of such asymmetries. In the **top-left panel**, the synthesised beam and scale bar are shown in the bottom-left and bottom-right corners, respectively. The colour bar to the right shows the colour scale in km s^{-1} . Coordinates are given as offsets (in arcseconds) relative to the image phase centre.

The idea that expanding radio jets can have an impact on the gaseous reservoirs on (sub-)kpc scales is relatively recent. Indeed, until some time ago, they were believed to operate mostly on the tens of kpc scale (by inflating cavities in the hot X-ray-emitting atmospheres of galaxies, groups, and clusters (see, e.g., [104])). Substantial recent work

on 3D hydrodynamical simulations of jet–ISM interactions has demonstrated that these can actually often occur on the circumnuclear regions of jetted AGN hosts, altering the gas physics, distribution, and kinematics at various levels (see [105–110] and references therein). These works indeed show that, while driving their way outward, the relativistic jet plasma can produce energy-driven bubbles that expand through the surrounding medium. The expanding bubbles can ablate the molecular gas clouds (i.e., locally compressing and/or fragmenting the gas distribution), accelerating them up to $\approx 1000 \text{ km s}^{-1}$ over a wide range of directions with respect to the jet axis and inducing shocks and turbulence into the cold molecular medium (thus yielding to higher gas excitation conditions; see also Section 2.1).

Over the past decade, thanks in particular to the advent of ALMA, such theoretical predictions have found support in a few confirmed examples of (sub-)kpc scale jet–ISM interactions (see [41,48,60,62,63,68,103,111,112]). A remarkable case in the context of this review is that of the nearby ($z = 0.011341$) lenticular galaxy IC 5063, hosting the young (i.e., $t_{\text{age}} \lesssim 1 \text{ Myr}$) core-double lobe radio source PKS 2048-57 observed at high resolution with ALMA in different molecular gas transitions (see [23,62,102]). These observations demonstrate a prominent alteration of the molecular gas kinematics in the regions co-spatial with the radio lobes, with anomalously high gas velocities (up to 650 km s^{-1}) that can be unequivocally explained as a jet-driven outflow with a mass rate of $\sim 12 M_{\odot} \text{ yr}^{-1}$ (see Figure 6, left panel). Molecular line ratios are also powerful tools to investigate the physical conditions of the gas in various environments, as different molecules, isotopologues, and transitions of the same species trace different gas components within the same galaxy. The ratios of the various molecular transitions observed in IC 5063 allow us to demonstrate that the molecular gas physics is modified around the radio source, varying from optically thick and sub-thermally excited in the unperturbed gas to optically thin with a high excitation temperature ($> 50 \text{ K}$) in the regions affected by the jet-driven outflow. Signs of gas fragmentation are also found, suggesting that the outflowing molecular gas is clumpy.

Another interesting (although less extreme) example is that of the radio galaxy PKS 0958–314, hosted by the local ($z = 0.0088$) lenticular galaxy NGC 3100 and detected at high resolution with ALMA in multiple CO transitions (up to $J_{\text{upper}} = 3$; see [34,41]). In this object, the ongoing jet–molecular gas coupling is inducing an outflow in the plane of the CO distribution, with $v_{\text{max}} \approx 200 \text{ km s}^{-1}$ and $\dot{M} \lesssim 0.12 M_{\odot} \text{ yr}^{-1}$. The interaction is also strongly altering the molecular gas physics by inducing very high CO line ratios and thus high gas excitation (with temperatures $T_{\text{ex}} \gtrsim 50 \text{ K}$) around the nuclear regions (see Figure 6, right panel). Other examples of local ETGs where it is confirmed that the presence of active radio jets is somehow altering the physics and kinematics of the molecular gas reservoirs on (sub-)kpc scales are NGC 1266 [113,114], NGC 1167 [115], and NGC 6328 [103,116].

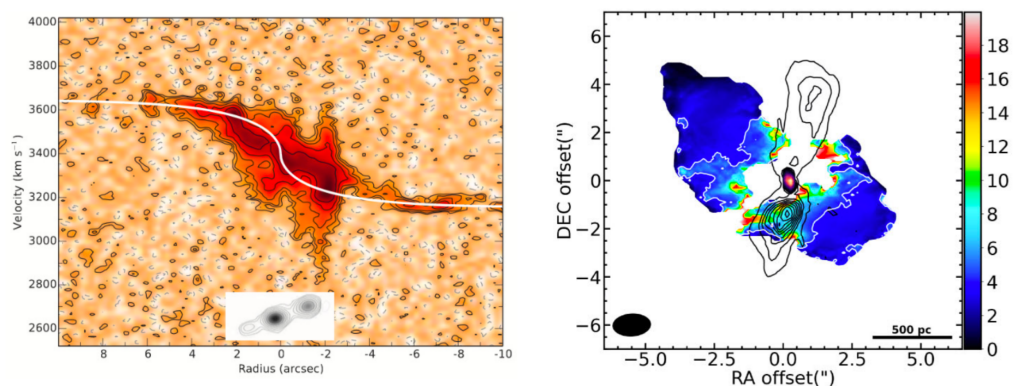


Figure 6. (Left panel) Major axis PVD of the CO(2-1) line emission observed with ALMA in the jetted AGN host IC 5063. The image is reproduced with permission from Morganti et al. [117]. The

white line represents the rotation curve derived from *Hubble Space Telescope* (HST) photometry and illustrates the expected kinematics of gas in regular circular rotation. The inset in the central bottom region shows the position and morphology of the core-double lobe radio structure as seen in the ALMA continuum at 230 GHz. **(Right panel)** $R_{21} \equiv S_{\text{CO}(2-1)}/S_{\text{CO}(1-0)}$ map of NGC 3100 with 10 GHz continuum contours of the core-double lobe radio structure overlaid in black. The map is reproduced from Ruffa et al. [41]. The white contour roughly marks the transition between the outer low-excitation component with $R_{21} < 4$ and the inner high-excitation component. The bar to the right shows the colour scale. The beam size and scale bar are shown in black in the bottom left and bottom right corners, respectively. Coordinates are given as relative to the image phase centre; east is to the left and north to the top.

The extent of jet-induced perturbations is predicted to vary depending mainly on the radio jet power and relative jet–gas orientation. In this scenario, jets of intermediate power ($P_{\text{jet}} \sim 10^{43}–10^{44} \text{ erg s}^{-1}$) at large ($\geq 45^\circ$) angles to the gas disc are predicted to interact more strongly and for longer times than jets of higher power ($P_{\text{jet}} > 10^{44} \text{ erg s}^{-1}$) oriented perpendicularly to the disc plane [107,108,118]. It has been also suggested that the strongest jet–ISM coupling (and thus the biggest impact on the gas physics *and* kinematics) occurs in the very early phases of the jet evolution (i.e., within less than 1 Myr from their launch), while the jets are still “trapped” within the dense nuclear gas layers [107,119]. The most extreme cases of the jet–ISM interactions mentioned above (and the few others in non-early-type hosts; see, e.g., [48,68]) have indeed all been caught in such an evolutionary phase of the jet, supporting this scenario. Once the jets break out from the dense nuclear regions and expand on larger scales, their impact should become progressively less extreme, and most of the gas affected by their transit is expected to eventually fall back into the central regions, settling into the galaxy potential on an estimated timescale on the order of tens of Myr (e.g., [118]). This would explain why, in presence of a 2 Myr-old radio source like the one hosted in NGC 3100, the jet-induced perturbations in the gas kinematics are much less extreme than in objects like IC 5063. At the same time, this picture makes it plausible that, when low-level disturbances compatible with a jet–ISM interaction are observed in systems with mature (large-scale) radio jets, we are actually observing the residual effects of a strong coupling that occurred in the past, with the gas still in the process of settling back into the potential well (see, e.g., [63]). The many details of these processes, however, have yet to be explored and thus remain unclear. Large samples of objects covering wide ranges of jet ages, powers, and jet–ISM relative orientation are required to gain a better understanding of the incidence and properties of jet–ISM interactions. This is essential information to fully assess the role of jet-induced feedback in galaxy evolution [119].

All of the properties illustrated above also apply to the few BCGs where the molecular gas has been observed to be settled in discs/rings onto the central (sub-)kpc scales (see, e.g., [33,54]). On the other hand, kpc-scale cold gas blobs and filaments associated with hot gas cooling flows and observed in the majority of BCGs are both predicted (e.g., [92]) and observed (e.g., [32,61,84,86,87,120]) to show very complex velocity patterns, with little or no evidence of regular rotation. This has been generally interpreted as an indication that the gas is not in a state of dynamical equilibrium in those cases, also showing signs of multiple and decoupled kinematic components (see, e.g., [37,120]). When the molecular gas in these systems is detected in absorption against a bright and compact background continuum source, evidence have been found that this traces inflowing cold molecular clouds that are moving toward the central SMBH with velocities up to 550 km s^{-1} , thus likely contributing to the fuelling of the jetted AGN (see, e.g., [24,27,35,47,54]).

In summary, while it is true that the bulk of the molecular gas detected in the majority of local ETGs is regularly rotating and dynamically cold, various localised levels of perturbations in the gas physics (i.e., high excitation conditions), morphology (e.g., warps, asymmetries, and/or disruptions) and kinematics (i.e., inflow/outflow motions) are ubiquitously detected in jetted AGN hosts. This clearly indicates that, when the central SMBH is caught in an active phase of its life, the gas is not fully relaxed into the host galaxy potential. All of this adds interesting clues to the potential connection between AGN

activity and the surrounding (sub-)kpc scale molecular gas discs and, more in general, to the interplay between the AGN and its host galaxy.

2.3. Gas Disc Stability: Star Formation and Black Hole Accretion

The molecular phase of the ISM is associated with active star formation, so that a rotating molecular gas disc/ring is generally expected to collapse into star-forming clouds. One may thus wonder how star formation proceeds in the gas-rich ETGs discussed above. To first order, these appear totally “dead” in—e.g.,—optical colour-magnitude diagrams because of their prominent red optical colours that barely differ from fully passive systems (see also Section 1). However, by using tracers that are more sensitive to star-forming regions (e.g., UV emission), some low-level star formation can also be picked out in these objects (e.g., [20,121]). The specific star formation rates ($sSFR \equiv SFR/M_*$) typically remain very low in such ETGs, because the gas reservoirs are small and embedded in a massive galaxy (e.g., [74]). They also have very low star-formation efficiencies ($SFE \equiv SFR/M_{H_2}$), for the obvious reason that the rates at which their molecular reservoirs form stars is modest compared to their masses (e.g., [74,122]). All this contributes to ensuring that gas-rich ETGs can still be considered overall “red and dead”.

The origin of this lowered star-formation efficiency in gas-rich ETGs is currently unclear. In general, the fate of cold gas distributions is governed by the balance between mechanisms that tend to gather molecular gas clouds together (such as self-gravity) and dissipative forces (e.g., shear and turbulence) that instead tend to pull them apart. As extensively discussed above, energetic feedback from an AGN (either in radiative or kinetic form) may be responsible for changing the physical conditions of the surrounding ISM by inducing shocks and turbulence, heating, compressing, or even expelling it from the nuclear regions through powerful outflows (e.g., [28,123,124]). This can either prevent gas fragmentation and thus successive bursts of star formation (negative feedback) or locally promote it (positive feedback; see, e.g., [81]). Thus, in the current scenario, AGN can play a crucial role in regulating the star formation activity of local gas-rich ETGs (e.g., [125]). At the same time, however, it has been shown that other factors may also intervene in these systems and influence the ability of their molecular gas to form stars (also because not all the SMBHs at the centre of local ETGs are currently caught in an active phase of their life).

ETGs are bulge-dominated systems, having very deep potential wells and thus very centrally concentrated stellar mass distributions. The circular velocity curves of this type of galaxy therefore rise sharply (as clearly visible also from the observed molecular gas velocity curves; see, e.g., Figures 4 and 5), leading to strong shear rates. Both observations and simulations have now shown that this, together with the strong gravitational influence exerted by the high-mass SMBHs typically hosted at their centres (see Section 3), have the effect of stabilising the cold gas against gravitational fragmentation, thus impacting the star-formation efficiency in these systems (see, e.g., [26,50,74,126,127]).

Historically, the local gas state against gravitational fragmentation has been quantitatively inferred from the analysis of the Toomre parameter [128]:

$$Q = \frac{\sigma_{\text{gas}} \kappa}{\pi G \Sigma_{\text{gas}}}, \quad (1)$$

where σ_{gas} and Σ_{gas} are the velocity dispersion and surface density, respectively, of the molecular gas, G is the gravitational constant, and κ is the epicyclic frequency (i.e., the frequency at which a gas parcel oscillates radially along its circular orbit). The latter is calculated as

$$\kappa = \sqrt{4\Omega^2 + R \frac{d\Omega^2}{dR}}, \quad (2)$$

where R is the radius of the gas distribution, and Ω is the angular frequency ($\Omega = v_{\text{circ}}/R$, with v_{circ} being the de-projected circular velocity). Theoretically, gas discs with Q values

above unity are considered stable against gravitational fragmentation, unstable otherwise. In the majority of the local ETGs where this type of analysis has been carried out, the average value of Q is found to be >1 (e.g., [25,26,34,73]). This, in first instance, provides some further support to a scenario in which the deep potentials of massive early-type hosts overall stabilise the gas distributions against gravitational collapse. However, caution is needed in drawing conclusions from the Toomre criterion alone, as $Q > 1$ have been measured in some nearby star-forming (disc) galaxies [129]. Numerical simulations also show that gravitational instabilities cannot be completely excluded in regions where Q is just slightly above unity [130]. Furthermore, observational and projection effects (such as those affecting the reliability of observed σ_{gas} values; see discussion at the beginning of Section 2.2) may also affect the estimation of Q (see, e.g., [34]). Therefore, a comprehensive analysis of the gas stability state and—more in general—of its star formation abilities requires highly-resolved (cloud-scale) CO observations (see e.g., [50]), as well as complementary data (such as spatially-resolved SFR maps) to directly detect star-forming regions.

Finally, we note that a stabilised gas state may also have important implications for the fuelling of the nuclear activity. High mass transfer rates and thus efficient SMBH accretion are indeed expected only if the gaseous circumnuclear matter is gravitationally unstable [131]. The fact that the molecular gas detected on the (sub-)kpc scales of local ETGs is overall found to be stable against gravitational fragmentation may thus also explain the low (or very low) rates of matter accretion onto the central SMBHs of some jetted AGN hosts (such as LERGs; see, e.g., [33,34,41,46]).

3. Measuring SMBH Masses from CO Kinematics

The last three decades of observations have demonstrated that the mass of central SMBHs (M_{BH}) correlates with a number of host galaxy properties, such as the bulge mass/luminosity (e.g., [132,133]) and the central stellar velocity dispersion (this latter being commonly indicated as the $M_{\text{BH}} - \sigma_{\star}$ relation; (e.g., [134–138])). This has been generally interpreted as implying a sort of self-regulated co-evolution between SMBHs and their host galaxies (e.g., [10]). In the current scenario, AGN feedback is typically invoked as a crucial element to set up such co-evolution, being responsible for altering the physics and kinematics of the ISM as described in Section 2. The many details of the mechanisms driving and regulating the SMBH–host galaxy interplay, however, are still poorly understood (see, e.g., [12] for a recent review).

One of the crucial steps to advance in our understanding of co-evolution is to pin down the SMBH–host galaxy correlations, as well as the true amount of their astrophysical scatter and its drivers. However, our ability to make such progress strongly depends on the accuracy of the M_{BH} measurements. The most reliable estimates are obtained through dynamical studies of matter orbiting within the sphere of influence (SOI) of the SMBH. This is the region inside which the gravitational potential of the SMBH dominates that of the host galaxy, and it is typically defined as $R_{\text{SOI}} = \frac{GM_{\text{BH}}}{\sigma_{\star}^2}$, where G is the gravitational constant, and σ_{\star} is the stellar velocity dispersion within one effective radius (see, e.g., [122]). Up until ~ 10 years ago, dynamical M_{BH} estimates were exclusively obtained by modelling the stellar (e.g., [139,140]), ionised gas (e.g., [141–144]), or megamaser kinematics (e.g., [145–147]) within R_{SOI} . Studies of the stellar kinematics can provide quite accurate M_{BH} estimates (with typical 1σ uncertainties $\lesssim 10\%$), but they can also be strongly affected by dust extinction and require very high resolution to reliably probe the line-of-sight stellar velocity distribution within the SOI. Dynamical measurements from ionised gas kinematics would be technically simpler, but they are often (if not always) challenged by the presence of non-gravitational forces (e.g., shocks) and/or turbulent gas motions superimposed on (quasi-)circular motion. Very high precision is usually achieved when using megamasers as tracers, as these typically probe material very close to the SMBH. However, megamaser emission is usually detected only in certain types of AGN (mostly Seyfert 2, typically in late-type hosts) and only if the megamaser disc is edge-on.

Over the past decade, thanks to the unprecedented resolution and sensitivity provided by ALMA, a new method for SMBH mass measurements has been developed: probing the kinematics of the molecular gas down to the SOI using CO emission lines (e.g., [25,29,30,39,46,52,53,96–98,148–152] and references therein). The basic assumption of this technique is that the kinematics of the molecular gas within the SOI mainly arises from the gravitational influence of both the luminous stellar component and the SMBH, this latter in particular giving rise to the characteristic Keplerian motions of matter orbiting around it (see Figure 7). Spatially resolving the Keplerian region thus allows us to constrain the SMBH mass to high accuracy, once the contribution of visible matter (i.e., the gas circular velocity component shown by the red dashed line in Figure 7) is removed from the the observed gas kinematics. A very recent work demonstrates that molecular gas observations of nearby galaxies using the most extended ALMA configurations can penetrate deep within the SOI, thus enabling SMBH mass estimates as precise as the best megamaser ones [153].

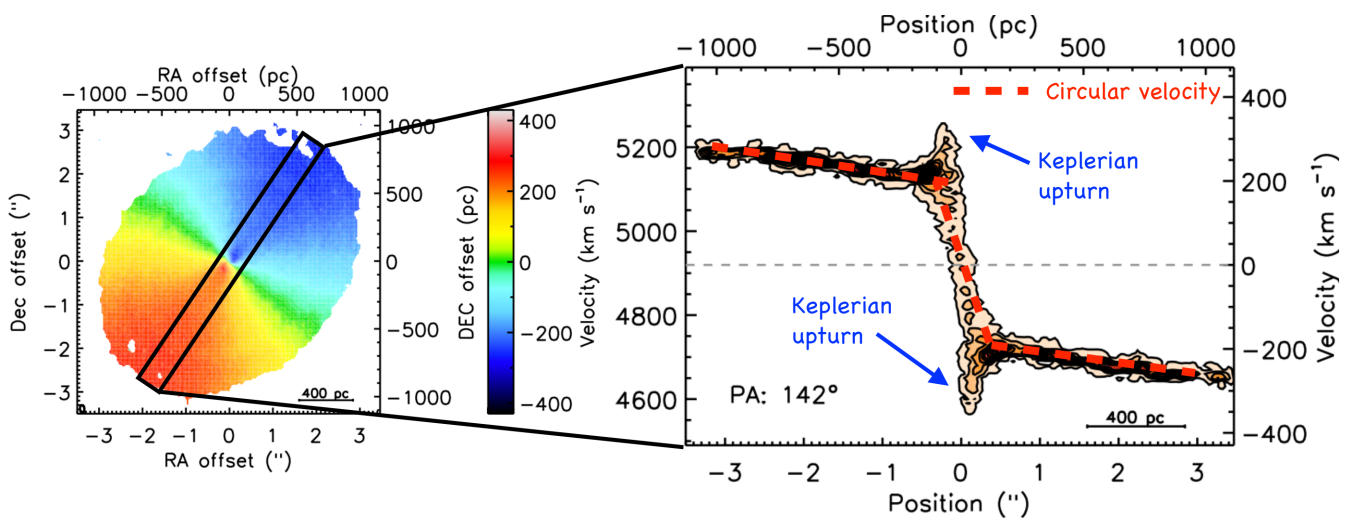


Figure 7. Diagram featuring the CO(2-1) moment 1 and PVD maps of the jetted AGN host NGC 383. Here, the resolution of the ALMA data allows us to resolve the R_{SOI} well and thus to clearly detect the characteristic Keplerian upturn (indicated by the blue arrows) of matter orbiting around a massive dark object. The maps are reproduced with permission from North et al. [30].

This technique has already been successfully applied to different types of galaxies (late- and early-types, active and inactive). However, given the molecular gas properties described in Section 2 (i.e., bulk of the gas regularly rotating and dynamically cold in most of the cases), ETGs are ideal targets to use the CO technique to dynamically measure SMBH masses with high accuracy. The presence of CO morphological asymmetries (e.g., warps) and/or nuclear gas deficiencies can be problematic, but it has already been demonstrated that reliable mass estimates can also be obtained in cases like these (e.g., [29,46,100,148,150]). Measuring SMBH masses using high-resolution ALMA CO observations in a diverse sample of galaxies is the primary aim of the mm-Wave Interferometric Survey of Dark Object Masses (WISDOM) project, which has to date provided accurate estimates in 10 typical ETGs of all types [25,29,30,46,53,100,148,150,151]. Other research groups carried out SMBH mass estimates for 13 additional ETGs [34,39,52,88,96–98,149,152,154]. This is enabling to either obtain accurate first constraints on the M_{BH} of these objects or robustly cross-check existing measurements that were previously derived using one of the techniques mentioned above (see, e.g., [39,46]).

In Figure 8, we present the $M_{\text{BH}} - \sigma_*$ relation from the compilation of van den Bosch [138], with the 23 SMBH mass measurements obtained so far by applying the molecular gas technique in ETGs overlaid as red dots. This plot overall shows that, while the majority of ETGs lie well within the scatter of the best-fitting relation (black line in Figure 8), a few

massive ones host SMBHs that lie towards the outer edge (or even slightly outside) of this scatter. This has been dubbed as the “over-massive” SMBH population (e.g., [155]). Galaxies within this class are thought to be local analogues of the higher-redshift quiescent galaxies that also contain over-massive black holes and could therefore be relics that have evolved little since a redshift $z \approx 2$ (e.g., [138]). Alternatively, an over-massive SMBH may be the result of merger(s), especially when paired with a high molecular gas mass in an ETG hosting an AGN. It is still not clear which of these scenarios best explains the observed behaviour. A recent work, however, suggests that over-massive SMBHs may in fact be fairly uncommon ($\lesssim 30\%$; [52]). Further work focusing on increasing the number of massive ETGs with accurate CO dynamical SMBH mass measurements will enable better constraints on the incidence of this population and—more in general—help us making further progress on our understanding of the high-mass end of the SMBH–host galaxy correlations.

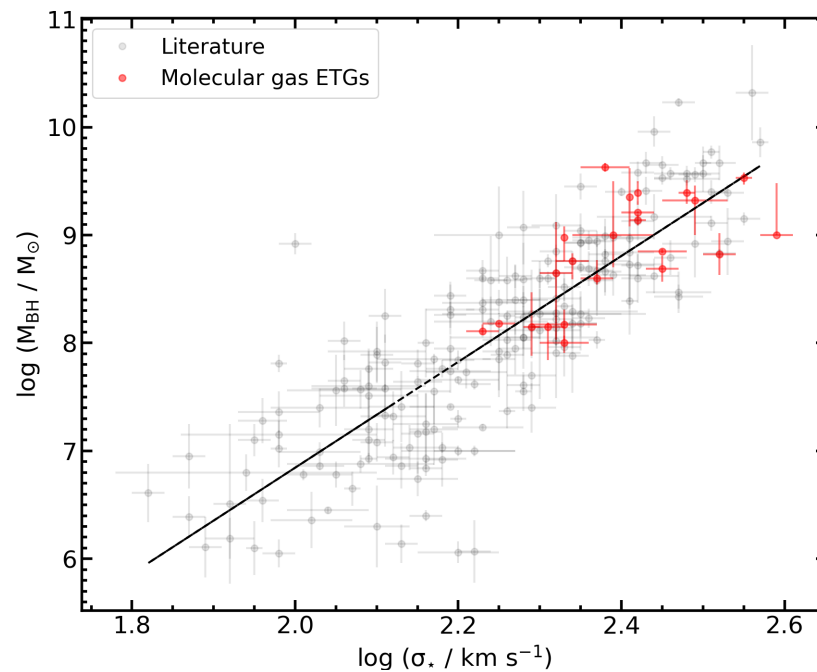


Figure 8. $M_{\text{BH}} - \sigma_*$ relationship from the compilation of van den Bosch [138] (grey data points and black line). The SMBH mass measurements obtained in nearby ETGs from CO dynamical modelling are overlaid as red dots and are taken from Davis et al. [25], Smith et al. [29], North et al. [30], Ruffa et al. [34], Boizelle et al. [39], Ruffa et al. [46], Dominiak et al. [52], Dominiak et al. [53], Boizelle et al. [96], Kabasares et al. [97], Kabasares et al. [98], Davis et al. [100], Davis et al. [148], Barth et al. [149], Onishi et al. [150], Smith et al. [151], Cohn et al. [152], and Onishi et al. [154]. For CO dynamical SMBH measurements, the error bars correspond to 1σ uncertainties.

4. Summary and Future Perspectives

In this work, we have briefly discussed the main lessons learned from the first 10 years of ALMA observations of the molecular gas component in local ETGs, restricting our analysis to objects within $z \lesssim 0.05$ and making clear distinctions between normal (inactive) ETGs, jetted AGN hosts, and BCGs (typically also hosting a jetted AGN). The main takeaway points from our short review can be summarised as follows:

- **Molecular gas content and distribution.** Molecular gas reservoirs with masses $\gtrsim 10^7 M_{\odot}$ are found in $\approx 25\%$ of local ETGs. In the majority of normal ETGs and jetted AGN hosts (including some BCGs), these significant amounts of cold gas have been observed to be distributed in smooth, thin, disc-like structures, extending on scales from a few hundred parsecs to a few kpc around the nuclear galaxy regions. In $\approx 20\%$ of the cases, the gas presents circumnuclear holes, with sizes ranging from a few tens to a few hundreds of parsecs. The origin of these nuclear gas deficiencies is still debated

(they may be due to either radiative dissociation, high gas excitation conditions, or dynamical or mechanical effects). In the majority of BCGs, the same large amounts of molecular gas are typically detected in the form of kpc-scale filamentary or blob-like structures, which are consistent with expectations from cooling flows.

- **Molecular gas kinematics.** In normal ETGs, the molecular gas is typically found to be regularly rotating and dynamically cold (with average $\sigma_{\text{gas}} \sim 10\text{--}20 \text{ km s}^{-1}$). Departure from symmetry (such as inclination or velocity warps) and/or secondary kinematic components (such as inflow/outflow motions) are rare. This is generally interpreted as an indication of gas that is both dynamically and morphologically settled within the potential well of the host galaxy. In jetted AGN hosts, while the bulk of the molecular gas is still consistent with being settled, various levels of local perturbations in the gas physics (i.e., high excitation conditions), morphology (e.g., warps, asymmetries, and/or disruptions) and kinematics (e.g., inflow/outflow motions) are ubiquitously observed. In general, this indicates that, when the central SMBH is caught in an active phase of its life, the gas is not fully relaxed into the host galaxy potential. In a few cases, by carrying out a detailed multi-wavelength analysis (including ALMA observations of multiple molecular gas tracers), it has been clearly shown that such alterations have to be ascribed to a jet–ISM interaction on a (sub-)kpc scale. Clear evidence of cold gas inflows onto galactic centres have been also found in the BCGs with gas distributed in filamentary or blob-like structures, where the gas overall tends to show complex kinematics (with little or no evidence of regular rotation).
- **Gas disc stability.** Even when hosting large amounts of cold molecular gas in their central regions, local ETGs remain overall “red and dead”. AGN feedback (in either radiative or kinetic form) can clearly play a role in maintaining them in this state. However, both simulations and high-resolution (i.e., a few tens of pc) ALMA observations have now shown that it is likely the strong shear rate induced by their deep potentials the dominant mechanism that stabilises the gas against gravitational collapse (thus hampering the formation of new stars). The fact that the molecular gas detected on the (sub-)kpc scale of local ETGs is overall found to be stable against gravitational fragmentation may also explain the low (or very low) rates of matter accretion onto the central SMBHs of some jetted AGN hosts (such as LERGs).
- **CO dynamical SMBH masses.** Before the advent of ALMA, dynamical estimates of the SMBH mass relied exclusively on studies of the stellar, ionised gas, and megamaser kinematics within the SMBH gravitational sphere of influence (R_{SOI}). Over the past decade, thanks to the ability of the most extended ALMA configurations to penetrate deep within the SOI, a new method for SMBH mass measurements has been developed and successfully applied to a varied range of galaxy types: probing the Keplerian motion of the molecular gas within the SOI using CO emission lines. Thanks to their molecular gas properties, ETGs are ideal targets for these types of studies. This is allowing us to put solid constraints on the high-mass ends of SMBH–host galaxy correlations (such as the $M_{\text{BH}} - \sigma_*$), and will ultimately help us make further progress in our understanding of the SMBH–host galaxy interplay (so-called co-evolution).

In short, it is clear that the first 10 years of ALMA observations have enabled transformative studies of the cold molecular phase of the ISM in nearby ETGs, allowing us to map its distribution and kinematics with unprecedented detail and thus to reveal some crucial aspects of the complex physics governing its survival and fate. This is in turn adding essential pieces of knowledge to our understanding of local galaxy populations and of the dark monsters hosted at their centres, and will ultimately help us to shed light on some longstanding debates about their observed properties.

Thanks to the latest and next-generation radio and optical telescopes, whose exquisite capabilities complement those of ALMA in the (sub-)mm range, we are already in a new exciting era for these types of studies. A comprehensive view of the cold ISM in local ETGs indeed requires also gathering detailed information on the atomic gas and the dust components. The former provides the material from which the molecular medium can

form and is typically traced by the atomic hydrogen (HI) hyper-fine transition at wavelengths of 21 cm (1.4 GHz). This can be found in both the circumnuclear and circumgalactic regions of ETGs in the form of diffuse structures, which can have very low column densities (i.e., $N_{\text{HI}} \lesssim 10^{19} \text{ cm}^{-2}$) and therefore require very high sensitivities to be detected (e.g., [156,157]). The South African SKA pathfinder (MeerKAT) is currently the best-suited instrument for these kinds of studies and is already allowing major steps forward in the field (see, e.g., [158]). Thanks to its 1.35× and 2× higher sensitivity and resolution, respectively, the planned MeerKAT extension (known as MeerKAT+) will soon allow us to achieve unprecedented performance in both cases, laying the groundwork for the full Square Kilometre Array (SKA) revolution.

Cold dust grains and, in particular, polycyclic aromatic hydrocarbons (PAHs) play a crucial role in a variety of processes within the ISM. For instance, they provide the surface for the formation of molecular hydrogen (H_2) and are responsible for the photoelectric heating of neutral gas. PAHs also absorb up to 20% of the UV light from young stars, re-emitting it in the near- and mid-infrared. This makes them promising, alternative tracers of star formation and total molecular gas mass. Furthermore, when spatially-resolved information on the cold dust is compared with that of molecular gas, it is possible to set crucial constraints on the origin of the cold ISM (see, e.g., [34,41]). Together with the information obtained from HI studies, this can provide a full and comprehensive picture of the cold ISM in massive quiescent galaxies. The James Webb Space Telescope (JWST) has already made strides in advancing our understanding of the dust component in nearby star-forming galaxies, and it is expected to allow for the same advances for ETGs (where the cold dust properties are currently poorly constrained).

Finally, it is also worth mentioning that, about 10 years from now, the next-generation Very Large Array (ngVLA) is expected to commence its full scientific operations. This will enable studies in the local Universe that will be complementary to those of both ALMA and SKA in terms of frequency coverage, but with much higher sensitivity and resolution (~10× higher sensitivity at 3 mm and baselines ~60× longer than ALMA). At the same time, it will allow us to reveal the details of the molecular gas component in the high-redshift (i.e., $z \gtrsim 1$) counterpart of local ETGs and their progenitor DSFGs, therefore making possible a full comprehension of the evolutionary track of massive spheroids.

All of the above will allow us to build up an increasingly complete observational picture of red sequence galaxies. Once meaningfully coupled with high-resolution simulations and appropriate theoretical models, this will clearly enable major steps forward in our understanding of this galaxy population.

Author Contributions: I.R. and T.A.D. contributed jointly to the literature research underlying this work and to the writing of the manuscript. All authors have read and agreed to the published version of the manuscript.

Funding: The research underlying this article was funded by grant #ST/S00033X/1 through the UK Science and Technology Facilities Council (STFC).

Data Availability Statement: All of the data discussed in this review are available to download at the ALMA Science Archive (<https://almascience.nrao.edu/asax/> (accessed on 20 June 2024)).

Acknowledgments: This review is mostly based on the contribution I.R. presented at the “Fifth Workshop on Millimetre Astronomy” (Bologna, Italy, May 2023). This paper makes use of ALMA data. ALMA is a partnership of ESO (representing its member states), NSF (USA), and NINS (Japan), together with NRC (Canada), NSC and ASIAA (Taiwan), and KASI (Republic of Korea), in cooperation with the Republic of Chile. The Joint ALMA Observatory is operated by ESO, AUI/NRAO, and NAOJ. This paper has also made use of the NASA/IPAC Extragalactic Database (NED), which is operated by the Jet Propulsion Laboratory, California Institute of Technology, under contract with NASA. We also acknowledge the use of the HyperLeda database (<http://leda.univ-lyon1.fr> (accessed on 20 June 2024)).

Conflicts of Interest: The authors declare no conflict of interest.

References

1. York, D.G.; Adelman, J.; Anderson, J.E., Jr.; Anderson, S.F.; Annis, J.; Bahcall, N.A.; Bakken, J.A.; Barkhouser, R.; Bastian, S.; Berman, E. The Sloan Digital Sky Survey: Technical Summary. *Astron. J.* **2000**, *120*, 1579–1587. [[CrossRef](#)]
2. Baldry, I.K.; Glazebrook, K.; Brinkmann, J.; Ivezić, Ž.; Lupton, R.H.; Nichol, R.C.; Szalay, A.S. Quantifying the Bimodal Color-Magnitude Distribution of Galaxies. *Astrophys. J.* **2004**, *600*, 681–694. [[CrossRef](#)]
3. Schiminovich, D.; Wyder, T.K.; Martin, D.C.; Johnson, B.D.; Salim, S.; Seibert, M.; Treyer, M.A.; Budavári, T.; Hoopes, C.; Zamojski, M.; et al. The UV-Optical Color Magnitude Diagram. II. Physical Properties and Morphological Evolution on and off of a Star-forming Sequence. *ApJS* **2007**, *173*, 315–341. [[CrossRef](#)]
4. Lapi, A.; Pantoni, L.; Zanisi, L.; Shi, J.; Mancuso, C.; Massardi, M.; Shankar, F.; Bressan, A.; Danese, L. The Dramatic Size and Kinematic Evolution of Massive Early-type Galaxies. *Astrophys. J.* **2018**, *857*, 22. [[CrossRef](#)]
5. Pantoni, L.; Lapi, A.; Massardi, M.; Goswami, S.; Danese, L. New Analytic Solutions for Galaxy Evolution: Gas, Stars, Metals, and Dust in Local ETGs and Their High-z Star-forming Progenitors. *Astrophys. J.* **2019**, *880*, 129. [[CrossRef](#)]
6. Giulietti, M.; Lapi, A.; Massardi, M.; Behiri, M.; Torsello, M.; D’Amato, Q.; Ronconi, T.; Perrotta, F.; Bressan, A. ALMA Resolves the First Strongly Lensed Optical/Near-IR-dark Galaxy. *Astrophys. J.* **2023**, *943*, 151. [[CrossRef](#)]
7. Salim, S.; Rich, R.M.; Charlot, S.; Brinchmann, J.; Johnson, B.D.; Schiminovich, D.; Seibert, M.; Mallery, R.; Heckman, T.M.; Forster, K.; et al. UV Star Formation Rates in the Local Universe. *Astrophys. J. Suppl. Ser.* **2007**, *173*, 267–292. [[CrossRef](#)]
8. Faber, S.M.; Willmer, C.N.A.; Wolf, C.; Koo, D.C.; Weiner, B.J.; Newman, J.A.; Im, M.; Coil, A.L.; Conroy, C.; Cooper, M.C.; et al. Galaxy Luminosity Functions to $z \sim 1$ from DEEP2 and COMBO-17: Implications for Red Galaxy Formation. *Astrophys. J.* **2007**, *665*, 265–294. [[CrossRef](#)]
9. Lilly, S.J.; Carollo, C.M.; Pipino, A.; Renzini, A.; Peng, Y. Gas Regulation of Galaxies: The Evolution of the Cosmic Specific Star Formation Rate, the Metallicity-Mass-Star-formation Rate Relation, and the Stellar Content of Halos. *Astrophys. J.* **2013**, *772*, 119. [[CrossRef](#)]
10. Kormendy, J.; Ho, L.C. Coevolution (or Not) of Supermassive Black Holes and Host Galaxies. *Annu. Rev. Astron. Astrophys.* **2013**, *51*, 511–653. [[CrossRef](#)]
11. Hardcastle, M. Interpreting radiative efficiency in radio-loud AGNs. *Nat. Astr.* **2018**, *2*, 273–274. [[CrossRef](#)]
12. D’Onofrio, M.; Marziani, P.; Chiosi, C. Past, Present and Future of the Scaling Relations of Galaxies and Active Galactic Nuclei. *Front. Astron. Space Sci.* **2021**, *8*, 157. [[CrossRef](#)]
13. Knapp, G.R.; Rupen, M.P. Molecular Gas in Elliptical Galaxies: CO Observations of an IRAS Flux-limited Sample. *Astrophys. J.* **1996**, *460*, 271. [[CrossRef](#)]
14. Welch, G.A.; Sage, L.J. The Cool Interstellar Medium in S0 Galaxies. I. A Survey of Molecular Gas. *Astrophys. J.* **2003**, *584*, 260–277. [[CrossRef](#)]
15. Combes, F.; Young, L.M.; Bureau, M. Molecular gas and star formation in the SAURON early-type galaxies. *Mon. Not. R. Astron. Soc.* **2007**, *377*, 1795–1807. [[CrossRef](#)]
16. Sage, L.J.; Welch, G.A.; Young, L.M. The Cool ISM in Elliptical Galaxies. I. A Survey of Molecular Gas. *Astrophys. J.* **2007**, *657*, 232–240. [[CrossRef](#)]
17. Young, L.M.; Bureau, M.; Cappellari, M. Structure and Kinematics of Molecular Disks in Fast-Rotator Early-Type Galaxies. *Astrophys. J.* **2008**, *676*, 317–334. [[CrossRef](#)]
18. Welch, G.A.; Sage, L.J.; Young, L.M. The Cool Interstellar Medium in Elliptical Galaxies. II. Gas Content in the Volume-limited Sample and Results from the Combined Elliptical and Lenticular Surveys. *Astrophys. J.* **2010**, *725*, 100–114. [[CrossRef](#)]
19. Young, L.M.; Bureau, M.; Davis, T.A.; Combes, F.; McDermid, R.M.; Alatalo, K.; Blitz, L.; Bois, M.; Bournaud, F.; Cappellari, M.; et al. The ATLAS^{3D} project—IV. The molecular gas content of early-type galaxies. *Mon. Not. R. Astron. Soc.* **2011**, *414*, 940–967. [[CrossRef](#)]
20. Crocker, A.F.; Bureau, M.; Young, L.M.; Combes, F. Molecular gas and star formation in early-type galaxies. *Mon. Not. R. Astron. Soc.* **2011**, *410*, 1197–1222. [[CrossRef](#)]
21. Alatalo, K.; Davis, T.A.; Bureau, M.; Young, L.M.; Blitz, L.; Crocker, A.F.; Bayet, E.; Bois, M.; Bournaud, F.; Cappellari, M.; et al. The ATLAS^{3D} project—XVIII. CARMA CO imaging survey of early-type galaxies. *Mon. Not. R. Astron. Soc.* **2013**, *432*, 1796–1844. [[CrossRef](#)]
22. Davis, T.A.; Greene, J.E.; Ma, C.P.; Blakeslee, J.P.; Dawson, J.M.; Pandya, V.; Veale, M.; Zabel, N. The MASSIVE survey—XI. What drives the molecular gas properties of early-type galaxies. *Mon. Not. R. Astron. Soc.* **2019**, *486*, 1404–1423. [[CrossRef](#)]
23. Morganti, R.; Oosterloo, T.; Oonk, J.B.R.; Frieswijk, W.; Tadhunter, C. The fast molecular outflow in the Seyfert galaxy IC 5063 as seen by ALMA. *Astron. Astrophys.* **2015**, *580*, A1. [[CrossRef](#)]
24. Tremblay, G.R.; Oonk, J.B.R.; Combes, F.; Salomé, P.; O’Dea, C.P.; Baum, S.A.; Voit, G.M.; Donahue, M.; McNamara, B.R.; Davis, T.A.; et al. Cold, clumpy accretion onto an active supermassive black hole. *Nature* **2016**, *534*, 218–221. [[CrossRef](#)]
25. Davis, T.A.; Bureau, M.; Onishi, K.; Cappellari, M.; Iguchi, S.; Sarzi, M. WISDOM Project—II. Molecular gas measurement of the supermassive black hole mass in NGC 4697. *Mon. Not. R. Astron. Soc.* **2017**, *468*, 4675–4690. [[CrossRef](#)]
26. Boizelle, B.D.; Barth, A.J.; Darling, J.; Baker, A.J.; Buote, D.A.; Ho, L.C.; Walsh, J.L. ALMA Observations of Circumnuclear Disks in Early-type Galaxies: ¹²CO(2-1) and Continuum Properties. *Astrophys. J.* **2017**, *845*, 170. [[CrossRef](#)]
27. Maccagni, F.M.; Morganti, R.; Oosterloo, T.A.; Oonk, J.B.R.; Emonts, B.H.C. ALMA observations of AGN fuelling. The case of PKS B1718-649. *Astron. Astrophys.* **2018**, *614*, A42. [[CrossRef](#)]

28. Harrison, C.M.; Costa, T.; Tadhunter, C.N.; Flütsch, A.; Kakkad, D.; Perna, M.; Vietri, G. AGN outflows and feedback twenty years on. *Nat. Astr.* **2018**, *2*, 198–205. [[CrossRef](#)]
29. Smith, M.D.; Bureau, M.; Davis, T.A.; Cappellari, M.; Liu, L.; North, E.V.; Onishi, K.; Iguchi, S.; Sarzi, M. WISDOM project—IV. A molecular gas dynamical measurement of the supermassive black hole mass in NGC 524. *Mon. Not. R. Astron. Soc.* **2019**, *485*, 4359–4374. [[CrossRef](#)]
30. North, E.V.; Davis, T.A.; Bureau, M.; Cappellari, M.; Iguchi, S.; Liu, L.; Onishi, K.; Sarzi, M.; Smith, M.D.; Williams, T.G. WISDOM project—V. Resolving molecular gas in Keplerian rotation around the supermassive black hole in NGC 0383. *Mon. Not. R. Astron. Soc.* **2019**, *490*, 319–330. [[CrossRef](#)]
31. Sansom, A.E.; Glass, D.H.W.; Bendo, G.J.; Davis, T.A.; Rowlands, K.; Bourne, N.; Dunne, L.; Eales, S.; Kaviraj, S.; Popescu, C.; et al. ALMA observations of massive molecular gas reservoirs in dusty early-type galaxies. *Mon. Not. R. Astron. Soc.* **2019**, *482*, 4617–4629. [[CrossRef](#)]
32. Olivares, V.; Salome, P.; Combes, F.; Hamer, S.; Guillard, P.; Lehnert, M.D.; Polles, F.L.; Beckmann, R.S.; Dubois, Y.; Donahue, M.; et al. Ubiquitous cold and massive filaments in cool core clusters. *Astron. Astrophys.* **2019**, *631*, A22. [[CrossRef](#)]
33. Ruffa, I.; Prandoni, I.; Laing, R.A.; Paladino, R.; Parma, P.; de Ruiter, H.; Mignano, A.; Davis, T.A.; Bureau, M.; Warren, J. The AGN fuelling/feedback cycle in nearby radio galaxies I. ALMA observations and early results. *Mon. Not. R. Astron. Soc.* **2019**, *484*, 4239–4259. [[CrossRef](#)]
34. Ruffa, I.; Davis, T.A.; Prandoni, I.; Laing, R.A.; Paladino, R.; Parma, P.; de Ruiter, H.; Casasola, V.; Bureau, M.; Warren, J. The AGN fuelling/feedback cycle in nearby radio galaxies—II. Kinematics of the molecular gas. *Mon. Not. R. Astron. Soc.* **2019**, *489*, 3739–3757. [[CrossRef](#)]
35. Rose, T.; Edge, A.C.; Combes, F.; Gaspari, M.; Hamer, S.; Nesvadba, N.; Peck, A.B.; Sarazin, C.; Tremblay, G.R.; Baum, S.A.; et al. Constraining cold accretion on to supermassive black holes: Molecular gas in the cores of eight brightest cluster galaxies revealed by joint CO and CN absorption. *Mon. Not. R. Astron. Soc.* **2019**, *489*, 349–365. [[CrossRef](#)]
36. Morokuma-Matsui, K.; Serra, P.; Maccagni, F.M.; For, B.Q.; Wang, J.; Bekki, K.; Morokuma, T.; Egusa, F.; Espada, D.; Miura, R.E.; et al. Complex distribution and velocity field of molecular gas in NGC 1316 as revealed by the Morita Array of ALMA. *Publ. Astron. Soc. Jpn.* **2019**, *71*, 85. [[CrossRef](#)]
37. North, E.V.; Davis, T.A.; Bureau, M.; Gaspari, M.; Cappellari, M.; Iguchi, S.; Liu, L.; Onishi, K.; Sarzi, M.; Smith, M.D.; et al. WISDOM project—VIII. Multiscale feedback cycles in the brightest cluster galaxy NGC 0708. *Mon. Not. R. Astron. Soc.* **2021**, *503*, 5179–5192. [[CrossRef](#)]
38. Smith, M.D.; Bureau, M.; Davis, T.A.; Cappellari, M.; Liu, L.; Onishi, K.; Iguchi, S.; North, E.V.; Sarzi, M. WISDOM project—VI. Exploring the relation between supermassive black hole mass and galaxy rotation with molecular gas. *Mon. Not. R. Astron. Soc.* **2021**, *500*, 1933–1952. [[CrossRef](#)]
39. Boizelle, B.D.; Walsh, J.L.; Barth, A.J.; Buote, D.A.; Baker, A.J.; Darling, J.; Ho, L.C.; Cohn, J.; Kabasares, K.M. Black Hole Mass Measurements of Radio Galaxies NGC 315 and NGC 4261 Using ALMA CO Observations. *Astrophys. J.* **2021**, *908*, 19. [[CrossRef](#)]
40. Young, L.M.; Meier, D.S.; Bureau, M.; Crocker, A.; Davis, T.A.; Topal, S. The Evolution of NGC 7465 as Revealed by Its Molecular Gas Properties. *Astrophys. J.* **2021**, *909*, 98. [[CrossRef](#)]
41. Ruffa, I.; Prandoni, I.; Davis, T.A.; Laing, R.A.; Paladino, R.; Casasola, V.; Parma, P.; Bureau, M. The AGN fuelling/feedback cycle in nearby radio galaxies—IV. Molecular gas conditions and jet-ISM interaction in NGC 3100. *Mon. Not. R. Astron. Soc.* **2022**, *510*, 4485–4503. [[CrossRef](#)]
42. Young, L.M.; Meier, D.S.; Crocker, A.; Davis, T.A.; Topal, S. Down but Not Out: Properties of the Molecular Gas in the Stripped Virgo Cluster Early-type Galaxy NGC 4526. *Astrophys. J.* **2022**, *933*, 90. [[CrossRef](#)]
43. Glass, D.H.W.; Sansom, A.E.; Davis, T.A.; Popescu, C.C. Cool interstellar medium as an evolutionary tracer in ALMA-observed local dusty early-type galaxies. *Mon. Not. R. Astron. Soc.* **2022**, *517*, 5524–5540. [[CrossRef](#)]
44. Temi, P.; Gaspari, M.; Brighenti, F.; Werner, N.; Grossova, R.; Gitti, M.; Sun, M.; Amblard, A.; Simionescu, A. Probing Multiphase Gas in Local Massive Elliptical Galaxies via Multiwavelength Observations. *Astrophys. J.* **2022**, *928*, 150. [[CrossRef](#)]
45. Torresi, E.; Balmaverde, B.; Liuzzo, E.; Giovannini, G.; Paladino, R.; Baldi, R.D.; Boccardi, B.; Capetti, A.; Ciprini, S.; Dadina, M.; et al. Exploring the radio morphology-accretion mode link in radio galaxies at high energies. *Mem. Soc. Astron. Ital.* **2022**, *93*, 81. [[CrossRef](#)]
46. Ruffa, I.; Davis, T.A.; Cappellari, M.; Bureau, M.; Elford, J.; Iguchi, S.; Lelli, F.; Liang, F.H.; Liu, L.; Lu, A.; et al. WISDOM project—XIV. SMBH mass in the early-type galaxies NGC 0612, NGC 1574, and NGC 4261 from CO dynamical modelling. *Mon. Not. R. Astron. Soc.* **2023**, *522*, 6170–6195. [[CrossRef](#)]
47. Rose, T.; McNamara, B. R.; Combes, F.; Edge, A. C.; Fabian, A. C.; Gaspari, M.; Russell, H.; Salomé, P.; Tremblay, G.; Ferland, G. Does absorption against AGN reveal supermassive black hole accretion? *Mon. Not. R. Astron. Soc.* **2023**, *518*, 878–892. [[CrossRef](#)]
48. Audibert, A.; Ramos Almeida, C.; García-Burillo, S.; Combes, F.; Bischetti, M.; Meenakshi, M.; Mukherjee, D.; Bicknell, G.; Wagner, A.Y. Jet-induced molecular gas excitation and turbulence in the Teacup. *Astron. Astrophys.* **2023**, *671*, L12. [[CrossRef](#)]
49. Maccagni, F.M.; Ruffa, I.; Loni, A.; Prandoni, I.; Ragusa, R.; Kleiner, D.; Serra, P.; Iodice, E.; Spavone, M. The AGN fuelling/feedback cycle in nearby radio galaxies. V. The cold atomic gas of NGC 3100 and its group. *Astron. Astrophys.* **2023**, *675*, A59. [[CrossRef](#)]

50. Williams, T.G.; Bureau, M.; Davis, T.A.; Cappellari, M.; Choi, W.; Elford, J.S.; Iguchi, S.; Gensior, J.; Liang, F.H.; Lu, A.; et al. WISDOM Project—XVII. Beam-by-beam properties of the molecular gas in early-type galaxies. *Mon. Not. R. Astron. Soc.* **2023**, *525*, 4270–4298. [[CrossRef](#)]
51. Elford, J.S.; Davis, T.A.; Ruffa, I.; Bureau, M.; Cappellari, M.; Gensior, J.; Iguchi, S.; Liang, F.H.; Liu, L.; Lu, A.; et al. WISDOM Project—XVI. The link between circumnuclear molecular gas reservoirs and active galactic nucleus fuelling. *Mon. Not. R. Astron. Soc.* **2024**, *528*, 319–336. [[CrossRef](#)]
52. Dominiak, P.; Bureau, M.; Davis, T.A.; Ma, C.P.; Greene, J.E.; Gu, M. The MASSIVE survey—XIX. Molecular gas measurements of the supermassive black hole masses in the elliptical galaxies NGC 1684 and NGC 0997. *Mon. Not. R. Astron. Soc.* **2024**, *529*, 1597–1616. [[CrossRef](#)]
53. Dominiak, P.; Cappellari, M.; Bureau, M.; Davis, T.A.; Sarzi, M.; Ruffa, I.; Iguchi, S.; Williams, T.G.; Zhang, H. WISDOM Project—XXIV. Cross-checking supermassive black hole mass estimates from ALMA CO gas kinematics and SINFONI stellar kinematics in the galaxy NGC 4751. *arXiv* **2024**, arXiv:2404.11260. [[CrossRef](#)]
54. Rose, T.; McNamara, B.R.; Combes, F.; Edge, A.C.; McDonald, M.; O’Sullivan, E.; Russell, H.; Fabian, A.C.; Ferland, G.; Salome, P.; et al. Two distinct molecular cloud populations detected in massive galaxies. *arXiv* **2024**, arXiv:2403.03974. [[CrossRef](#)]
55. Jungwiert, B.; Combes, F.; Palouš, J. Continuous stellar mass-loss in N-body models of galaxies. *Astron. Astrophys.* **2001**, *376*, 85–97. [[CrossRef](#)]
56. Storchi-Bergmann, T.; Schnorr-Müller, A. Observational constraints on the feeding of supermassive black holes. *Nat. Astr.* **2019**, *3*, 48–61. [[CrossRef](#)]
57. Padovani, P. The faint radio sky: Radio astronomy becomes mainstream. *Astron. Astrophys. Rev.* **2016**, *24*, 13. [[CrossRef](#)]
58. Heckman, T.M.; Best, P.N. The Coevolution of Galaxies and Supermassive Black Holes: Insights from Surveys of the Contemporary Universe. *Annu. Rev. Astron. Astrophys.* **2014**, *52*, 589–660. [[CrossRef](#)]
59. Padovani, P.; Alexander, D.M.; Assef, R.J.; De Marco, B.; Giommi, P.; Hickox, R.C.; Richards, G.T.; Smolčić, V.; Hatziminaoglou, E.; Mainieri, V. Active galactic nuclei: What’s in a name? *Astron. Astrophys. Rev.* **2017**, *25*, 2. [[CrossRef](#)]
60. García-Burillo, S.; Combes, F.; Usero, A.; Aalto, S.; Krips, M.; Viti, S.; Alonso-Herrero, A.; Hunt, L.K.; Schinnerer, E.; Baker, A.J.; et al. Molecular line emission in NGC 1068 imaged with ALMA. I. An AGN-driven outflow in the dense molecular gas. *Astron. Astrophys.* **2014**, *567*, A125. [[CrossRef](#)]
61. Russell, H.R.; McNamara, B.R.; Fabian, A.C.; Nulsen, P.E.J.; Edge, A.C.; Combes, F.; Murray, N.W.; Parrish, I.J.; Salomé, P.; Sanders, J.S.; et al. ALMA observations of cold molecular gas filaments trailing rising radio bubbles in PKS 0745-191. *Mon. Not. R. Astron. Soc.* **2016**, *458*, 3134–3149. [[CrossRef](#)]
62. Oosterloo, T.; Raymond Oonk, J.B.; Morganti, R.; Combes, F.; Dasyra, K.; Salomé, P.; Vlahakis, N.; Tadhunter, C. Properties of the molecular gas in the fast outflow in the Seyfert galaxy IC 5063. *Astron. Astrophys.* **2017**, *608*, A38. [[CrossRef](#)]
63. Ruffa, I.; Laing, R.A.; Prandoni, I.; Paladino, R.; Parma, P.; Davis, T.A.; Bureau, M. The AGN fuelling/feedback cycle in nearby radio galaxies—III. 3D relative orientations of radio jets and CO discs and their interaction. *Mon. Not. R. Astron. Soc.* **2020**, *499*, 5719–5731. [[CrossRef](#)]
64. Dotti, M.; Buscicchio, R.; Bollati, F.; Decarli, R.; Del Pozzo, W.; Franchini, A. Partial alignment between jets and megamasers: Coherent or selective accretion? *arXiv* **2024**, arXiv:2403.18002. [[CrossRef](#)]
65. Best, P.N.; Heckman, T.M. On the fundamental dichotomy in the local radio-AGN population: Accretion, evolution and host galaxy properties. *Mon. Not. R. Astron. Soc.* **2012**, *421*, 1569–1582. [[CrossRef](#)]
66. Hardcastle, M.J.; Evans, D.A.; Croston, J.H. Hot and cold gas accretion and feedback in radio-loud active galaxies. *Mon. Not. R. Astron. Soc.* **2007**, *376*, 1849–1856. [[CrossRef](#)]
67. Bolatto, A.D.; Wolfire, M.; Leroy, A.K. The CO-to-H₂ Conversion Factor. *Annu. Rev. Astron. Astrophys.* **2013**, *51*, 207–268. [[CrossRef](#)]
68. Zovaro, H.R.M.; Sharp, R.; Nesvadba, N.P.H.; Bicknell, G.V.; Mukherjee, D.; Wagner, A.Y.; Groves, B.; Krishna, S. Jets blowing bubbles in the young radio galaxy 4C 31.04. *Mon. Not. R. Astron. Soc.* **2019**, *484*, 3393–3409. [[CrossRef](#)]
69. Carilli, C.L.; Walter, F. Cool Gas in High-Redshift Galaxies. *Annu. Rev. Astron. Astrophys.* **2013**, *51*, 105–161. [[CrossRef](#)]
70. Topal, S.; Bureau, M.; Davis, T.A.; Krips, M.; Young, L.M.; Crocker, A.F. Molecular gas kinematics and line diagnostics in early-type galaxies: NGC 4710 and NGC 5866. *Mon. Not. R. Astron. Soc.* **2016**, *463*, 4121–4152. [[CrossRef](#)]
71. Bigiel, F.; Leroy, A.K.; Jiménez-Donaire, M.J.; Pety, J.; Usero, A.; Cormier, D.; Bolatto, A.; García-Burillo, S.; Colombo, D.; González-García, M.; et al. The EMPIRE Survey: Systematic Variations in the Dense Gas Fraction and Star Formation Efficiency from Full-disk Mapping of M51. *Astrophys. J. Lett.* **2016**, *822*, L26. [[CrossRef](#)]
72. Ocaña Flaquer, B.; Leon, S.; Combes, F.; Lim, J. TANGO I: Interstellar medium in nearby radio galaxies. Molecular gas. *Astron. Astrophys.* **2010**, *518*, A9. [[CrossRef](#)]
73. Van de Voort, F.; Davis, T.A.; Matsushita, S.; Rowlands, K.; Shabala, S.S.; Allison, J.R.; Ting, Y.S.; Sansom, A.E.; van der Werf, P.P. An ALMA view of star formation efficiency suppression in early-type galaxies after gas-rich minor mergers. *Mon. Not. R. Astron. Soc.* **2018**, *476*, 1232. [[CrossRef](#)]
74. Davis, T.A.; Gensior, J.; Bureau, M.; Cappellari, M.; Choi, W.; Elford, J.S.; Kruijssen, J.M.D.; Lelli, F.; Liang, F.H.; Liu, L.; et al. WISDOM Project—X. The morphology of the molecular ISM in galaxy centres and its dependence on galaxy structure. *Mon. Not. R. Astron. Soc.* **2022**, *512*, 1522–1540. [[CrossRef](#)]

75. Davis, T.A.; Alatalo, K.; Bureau, M.; Cappellari, M.; Scott, N.; Young, L.M.; Blitz, L.; Crocker, A.; Bayet, E.; Bois, M.; et al. The ATLAS^{3D} Project—XIV. The extent and kinematics of the molecular gas in early-type galaxies. *Mon. Not. R. Astron. Soc.* **2013**, *429*, 534–555. [[CrossRef](#)]
76. Combes, F.; García-Burillo, S.; Audibert, A.; Hunt, L.; Eckart, A.; Aalto, S.; Casasola, V.; Boone, F.; Krips, M.; Viti, S.; et al. ALMA observations of molecular tori around massive black holes. *Astron. Astrophys.* **2019**, *623*, A79. [[CrossRef](#)]
77. García-Burillo, S.; Combes, F.; Ramos Almeida, C.; Usero, A.; Alonso-Herrero, A.; Hunt, L.K.; Rouan, D.; Aalto, S.; Querejeta, M.; Viti, S.; et al. ALMA images the many faces of the NGC 1068 torus and its surroundings. *Astron. Astrophys.* **2019**, *632*, A61. [[CrossRef](#)]
78. Imanishi, M.; Nakanishi, K. ALMA Observations of Nearby Luminous Infrared Galaxies with Various AGN Energetic Contributions Using Dense Gas Tracers. *Astron. J.* **2014**, *148*, 9. [[CrossRef](#)]
79. Imanishi, M.; Nakanishi, K.; Izumi, T.; Wada, K. ALMA Reveals an Inhomogeneous Compact Rotating Dense Molecular Torus at the NGC 1068 Nucleus. *Astrophys. J. Lett.* **2018**, *853*, L25. [[CrossRef](#)]
80. García-Burillo, S.; Alonso-Herrero, A.; Ramos Almeida, C.; González-Martín, O.; Combes, F.; Usero, A.; Hönig, S.; Querejeta, M.; Hicks, E.K.S.; Hunt, L.K.; et al. The Galaxy Activity, Torus, and Outflow Survey (GATOS). I. ALMA images of dusty molecular tori in Seyfert galaxies. *Astron. Astrophys.* **2021**, *652*, A98. [[CrossRef](#)]
81. Harrison, C.M.; Ramos Almeida, C. Observational Tests of Active Galactic Nuclei Feedback: An Overview of Approaches and Interpretation. *Galaxies* **2024**, *12*, 17. [[CrossRef](#)]
82. Combes, F. Dynamical Evolution: Spirals and Bars. In *Proceedings of the Galaxy Disks and Disk Galaxies, Rome, Italy, 12–16 June 2000*; Astronomical Society of the Pacific Conference Series; Funes, J.G., Corsini, E.M., Eds.; Astronomical Society of the Pacific: San Francisco, CA, USA, 2001; Volume 230, pp. 213–220.
83. Combes, F.; García-Burillo, S.; Casasola, V.; Hunt, L.; Krips, M.; Baker, A.J.; Boone, F.; Eckart, A.; Marquez, I.; Neri, R.; et al. ALMA observations of feeding and feedback in nearby Seyfert galaxies: An AGN-driven outflow in NGC 1433. *Astron. Astrophys.* **2013**, *558*, A124. [[CrossRef](#)]
84. David, L.P.; Lim, J.; Forman, W.; Vrtilik, J.; Combes, F.; Salome, P.; Edge, A.; Hamer, S.; Jones, C.; Sun, M.; et al. Molecular Gas in the X-ray Bright Group NGC 5044 as Revealed by ALMA. *Astrophys. J.* **2014**, *792*, 94. [[CrossRef](#)]
85. Werner, N.; Oonk, J.B.R.; Sun, M.; Nulsen, P.E.J.; Allen, S.W.; Canning, R.E.A.; Simionescu, A.; Hoffer, A.; Connor, T.; Donahue, M.; et al. The origin of cold gas in giant elliptical galaxies and its role in fuelling radio-mode AGN feedback. *Mon. Not. R. Astron. Soc.* **2014**, *439*, 2291–2306. [[CrossRef](#)]
86. Temi, P.; Amblard, A.; Gitti, M.; Brighenti, F.; Gaspari, M.; Mathews, W.G.; David, L. ALMA Observations of Molecular Clouds in Three Group-centered Elliptical Galaxies: NGC 5846, NGC 4636, and NGC 5044. *Astrophys. J.* **2018**, *858*, 17. [[CrossRef](#)]
87. Tremblay, G.R.; Combes, F.; Oonk, J.B.R.; Russell, H.R.; McDonald, M.A.; Gaspari, M.; Husemann, B.; Nulsen, P.E.J.; McNamara, B.R.; Hamer, S.L.; et al. A Galaxy-scale Fountain of Cold Molecular Gas Pumped by a Black Hole. *Astrophys. J.* **2018**, *865*, 13. [[CrossRef](#)]
88. Nagai, H.; Onishi, K.; Kawakatu, N.; Fujita, Y.; Kino, M.; Fukazawa, Y.; Lim, J.; Forman, W.; Vrtilik, J.; Nakanishi, K.; et al. The ALMA Discovery of the Rotating Disk and Fast Outflow of Cold Molecular Gas in NGC 1275. *Astrophys. J.* **2019**, *883*, 193. [[CrossRef](#)]
89. Gaspari, M.; Ruszkowski, M.; Oh, S.P. Chaotic cold accretion on to black holes. *Mon. Not. R. Astron. Soc.* **2013**, *432*, 3401–3422. [[CrossRef](#)]
90. King, A.; Nixon, C. AGN flickering and chaotic accretion. *Mon. Not. R. Astron. Soc.* **2015**, *453*, L46–L47. [[CrossRef](#)]
91. Gaspari, M.; Brighenti, F.; Temi, P. Chaotic cold accretion on to black holes in rotating atmospheres. *Astron. Astrophys.* **2015**, *579*, A62. [[CrossRef](#)]
92. Gaspari, M.; Temi, P.; Brighenti, F. Raining on black holes and massive galaxies: The top-down multiphase condensation model. *Mon. Not. R. Astron. Soc.* **2017**, *466*, 677–704. [[CrossRef](#)]
93. Babyk, I.V.; McNamara, B.R.; Tamhane, P.D.; Nulsen, P.E.J.; Russell, H.R.; Edge, A.C. Origins of Molecular Clouds in Early-type Galaxies. *Astrophys. J.* **2019**, *887*, 149. [[CrossRef](#)]
94. Di Teodoro, E.M.; Fraternali, F. ^{3D} BAROLO: A new 3D algorithm to derive rotation curves of galaxies. *Mon. Not. R. Astron. Soc.* **2015**, *451*, 3021–3033. [[CrossRef](#)]
95. Krajnović, D.; Cappellari, M.; de Zeeuw, P.T.; Copin, Y. Kinometry: A generalization of photometry to the higher moments of the line-of-sight velocity distribution. *Mon. Not. R. Astron. Soc.* **2006**, *366*, 787–802. [[CrossRef](#)]
96. Boizelle, B.D.; Barth, A.J.; Walsh, J.L.; Buote, D.A.; Baker, A.J.; Darling, J.; Ho, L.C. A Precision Measurement of the Mass of the Black Hole in NGC 3258 from High-resolution ALMA Observations of Its Circumnuclear Disk. *Astrophys. J.* **2019**, *881*, 10. [[CrossRef](#)]
97. Kabasares, K.M.; Barth, A.J.; Buote, D.A.; Boizelle, B.D.; Walsh, J.L.; Baker, A.J.; Darling, J.; Ho, L.C.; Cohn, J. Black Hole Mass Measurements of Early-type Galaxies NGC 1380 and NGC 6861 through ALMA and HST Observations and Gas-dynamical Modeling. *Astrophys. J.* **2022**, *934*, 162. [[CrossRef](#)]
98. Kabasares, K.M.; Cohn, J.H.; Barth, A.J.; Boizelle, B.D.; Davidson, J.; Sy, J.M.; Flores-Velázquez, J.; Delgado Andrade, S.C.; Buote, D.A.; Walsh, J.L.; et al. Gas-dynamical Mass Measurements of the Supermassive Black Holes in the Early-Type Galaxies NGC 4786 and NGC 5193 from ALMA and HST Observations. *arXiv* **2024**, arXiv:2403.00181. [[CrossRef](#)]

99. Cappellari, M.; Emsellem, E.; Krajnović, D.; McDermid, R.M.; Scott, N.; Verdoes Kleijn, G.A.; Young, L.M.; Alatalo, K.; Bacon, R.; Blitz, L.; et al. The ATLAS^{3D} project—I. A volume-limited sample of 260 nearby early-type galaxies: Science goals and selection criteria. *Mon. Not. R. Astron. Soc.* **2011**, *413*, 813–836. [[CrossRef](#)]
100. Davis, T.A.; Bureau, M.; Onishi, K.; van de Voort, F.; Cappellari, M.; Iguchi, S.; Liu, L.; North, E.V.; Sarzi, M.; Smith, M.D. WISDOM Project—III. Molecular gas measurement of the supermassive black hole mass in the barred lenticular galaxy NGC4429. *Mon. Not. R. Astron. Soc.* **2018**, *473*, 3818–3834. [[CrossRef](#)]
101. Wisnioski, E.; Förster Schreiber, N.M.; Wuyts, S.; Wuyts, E.; Bandara, K.; Wilman, D.; Genzel, R.; Bender, R.; Davies, R.; Fossati, M.; et al. The KMOS^{3D} Survey: Design, First Results, and the Evolution of Galaxy Kinematics from $0.7 \leq z \leq 2.7$. *Astrophys. J.* **2015**, *799*, 209. [[CrossRef](#)]
102. Dasyra, K.M.; Combes, F.; Oosterloo, T.; Oonk, J.B.R.; Morganti, R.; Salomé, P.; Vlahakis, N. ALMA reveals optically thin, highly excited CO gas in the jet-driven winds of the galaxy IC 5063. *Astron. Astrophys.* **2016**, *595*, L7. [[CrossRef](#)]
103. Papachristou, M.; Dasyra, K.M.; Fernández-Ontiveros, J.A.; Audibert, A.; Ruffa, I.; Combes, F.; Polkas, M.; Gkogkou, A. A plausible link between dynamically unsettled molecular gas and the radio jet in NGC 6328. *Astron. Astrophys.* **2023**, *679*, A115. [[CrossRef](#)]
104. McNamara, B.R.; Nulsen, P.E.J. Mechanical feedback from active galactic nuclei in galaxies, groups and clusters. *N. J. Phys.* **2012**, *14*, 055023. [[CrossRef](#)]
105. Wagner, A.Y.; Bicknell, G.V.; Umemura, M. Driving Outflows with Relativistic Jets and the Dependence of Active Galactic Nucleus Feedback Efficiency on Interstellar Medium Inhomogeneity. *Astrophys. J.* **2012**, *757*, 136. [[CrossRef](#)]
106. Wagner, A.Y.; Bicknell, G.V.; Umemura, M.; Sutherland, R.S.; Silk, J. Galaxy-scale AGN feedback—Theory. *Astron. Nachrichten* **2016**, *337*, 167. [[CrossRef](#)]
107. Mukherjee, D.; Wagner, A.Y.; Bicknell, G.V.; Morganti, R.; Oosterloo, T.; Nesvadba, N.; Sutherland, R.S. The jet-ISM interactions in IC 5063. *Mon. Not. R. Astron. Soc.* **2018**, *476*, 80–95. [[CrossRef](#)]
108. Mukherjee, D.; Bicknell, G.V.; Wagner, A.Y.; Sutherland, R.S.; Silk, J. Relativistic jet feedback—III. Feedback on gas discs. *Mon. Not. R. Astron. Soc.* **2018**, *479*, 5544–5566. [[CrossRef](#)]
109. Cielo, S.; Bieri, R.; Volonteri, M.; Wagner, A.Y.; Dubois, Y. AGN feedback compared: Jets versus radiation. *Mon. Not. R. Astron. Soc.* **2018**, *477*, 1336–1355. [[CrossRef](#)]
110. Mukherjee, D.; Bicknell, G.V.; Wagner, A.Y. Resolved simulations of jet–ISM interaction: Implications for gas dynamics and star formation. *Astron. Nachrichten* **2021**, *342*, 1140–1145. [[CrossRef](#)]
111. Dasyra, K.M.; Bostrom, A.C.; Combes, F.; Vlahakis, N. A Radio Jet Drives a Molecular and Atomic Gas Outflow in Multiple Regions within One Square Kiloparsec of the Nucleus of the nearby Galaxy IC5063. *Astrophys. J.* **2015**, *815*, 34. [[CrossRef](#)]
112. Murthy, S.; Morganti, R.; Oosterloo, T.; Schulz, R.; Mukherjee, D.; Wagner, A.Y.; Bicknell, G.; Prandoni, I.; Shulevski, A.a. Feedback from low-luminosity radio galaxies: B2 0258+35. *Astron. Astrophys.* **2019**, *629*, A58. [[CrossRef](#)]
113. Alatalo, K.; Blitz, L.; Young, L.M.; Davis, T.A.; Bureau, M.; Lopez, L.A.; Cappellari, M.; Scott, N.; Shapiro, K.L.; Crocker, A.F.; et al. Discovery of an Active Galactic Nucleus Driven Molecular Outflow in the Local Early-type Galaxy NGC 1266. *Astrophys. J.* **2011**, *735*, 88. [[CrossRef](#)]
114. Nyland, K.; Alatalo, K.; Wrobel, J.M.; Young, L.M.; Morganti, R.; Davis, T.A.; de Zeeuw, P.T.; Deustua, S.; Bureau, M. Detection of a High Brightness Temperature Radio Core in the Active-galactic-nucleus-driven Molecular Outflow Candidate NGC 1266. *Astrophys. J.* **2013**, *779*, 173. [[CrossRef](#)]
115. Murthy, S.; Morganti, R.; Wagner, A.Y.; Oosterloo, T.; Guillard, P.; Mukherjee, D.; Bicknell, G. Cold gas removal from the centre of a galaxy by a low-luminosity jet. *Nature Astr.* **2022**, *6*, 488–495. [[CrossRef](#)]
116. Papachristou, M.; Dasyra, K.M.; Fernández-Ontiveros, J.A.; Audibert, A.; Ruffa, I.; Combes, F. CO kinematics unveil outflows plausibly driven by a young jet in the gigahertz peaked radio core of NGC 6328. *Astron. Nachrichten* **2021**, *342*, 1160–1165. [[CrossRef](#)]
117. Morganti, R.; Oosterloo, T.A.; Oonk, J.B.R.; Frieswijk, W.; Tadhunter, C.N. Radio Jets Clearing the Way Through a Galaxy: Watching Feedback in Action in the Seyfert Galaxy IC 5063. In *Proceedings of the Revolution in Astronomy with ALMA: The Third Year, Tokyo, Japan, 8–11 December 2014*; Astronomical Society of the Pacific Conference Series; Iono, D., Tatematsu, K., Wootten, A., Testi, L., Eds.; Astronomical Society of the Pacific: San Francisco, CA, USA, 2015; Volume 499, p. 125. [[CrossRef](#)]
118. Mukherjee, D.; Bicknell, G.V.; Sutherland, R.; Wagner, A. Relativistic jet feedback in high-redshift galaxies—I. Dynamics. *Mon. Not. R. Astron. Soc.* **2016**, *461*, 967–983. [[CrossRef](#)]
119. Morganti, R.; Oosterloo, T.; Tadhunter, C.N. Taking snapshots of the jet-ISM interplay with ALMA. In *Proceedings of the Galaxy Evolution and Feedback across Different Environments, Bento Gonçalves, Brazil, 2–6 March 2020*; Storchi Bergmann, T., Forman, W., Overzier, R., Riffel, R., Eds.; Cambridge University Press, Cambridge, UK, 2021; Volume 359, pp. 243–248. [[CrossRef](#)]
120. Oosterloo, T.; Morganti, R.; Murthy, S. Closing the feedback-feeding loop of the radio galaxy 3C 84. *Nature Astr.* **2024**, *8*, 256–262. [[CrossRef](#)]
121. Young, L.M.; Scott, N.; Serra, P.; Alatalo, K.; Bayet, E.; Blitz, L.; Bois, M.; Bournaud, F.; Bureau, M.; Crocker, A.F.; et al. The ATLAS^{3D} project—XXVII. Cold gas and the colours and ages of early-type galaxies. *Mon. Not. R. Astron. Soc.* **2014**, *444*, 3408–3426. [[CrossRef](#)]
122. Davis, T.A. A figure of merit for black hole mass measurements with molecular gas. *Mon. Not. R. Astron. Soc.* **2014**, *443*, 911–918. [[CrossRef](#)]

123. Combes, F. AGN feedback and its quenching efficiency. *Front. Astron. Space Sci.* **2017**, *4*, 10. [[CrossRef](#)]
124. Morganti, R.; Oosterloo, T.; Tadhunter, C.N. Taking snapshots of the jet-ISM interplay with ALMA. *arXiv* **2020**, arXiv:2005.04765.
125. Choi, E.; Ostriker, J.P.; Naab, T.; Oser, L.; Moster, B.P. The impact of mechanical AGN feedback on the formation of massive early-type galaxies. *Mon. Not. R. Astron. Soc.* **2015**, *449*, 4105–4116. [[CrossRef](#)]
126. Martig, M.; Crocker, A.F.; Bournaud, F.; Emsellem, E.; Gabor, J.M.; Alatalo, K.; Blitz, L.; Bois, M.; Bureau, M.; Cappellari, M.; et al. The ATLAS^{3D} project—XXII. Low-efficiency star formation in early-type galaxies: Hydrodynamic models and observations. *Mon. Not. R. Astron. Soc.* **2013**, *432*, 1914–1927. [[CrossRef](#)]
127. Davis, T.A.; Young, L.M.; Crocker, A.F.; Bureau, M.; Blitz, L.; Alatalo, K.; Emsellem, E.; Naab, T.; Bayet, E.; Bois, M.; et al. The ATLAS^{3D} Project—XXVIII. Dynamically driven star formation suppression in early-type galaxies. *Mon. Not. R. Astron. Soc.* **2014**, *444*, 3427–3445. [[CrossRef](#)]
128. Toomre, A. On the gravitational stability of a disk of stars. *Astrophys. J.* **1964**, *139*, 1217–1238. [[CrossRef](#)]
129. Romeo, A.B.; Mogotsi, K.M. What drives gravitational instability in nearby star-forming spirals? The impact of CO and H I velocity dispersions. *Mon. Not. R. Astron. Soc.* **2017**, *469*, 286–294. [[CrossRef](#)]
130. Li, Y.; Mac Low, M.M.; Klessen, R.S. Star Formation in Isolated Disk Galaxies. I. Models and Characteristics of Nonlinear Gravitational Collapse. *Astrophys. J.* **2005**, *626*, 823–843. [[CrossRef](#)]
131. Wada, K.; Habe, A. Rapid gas supply to a nuclear region by self-gravitational instability in a weak barred potential. *Mon. Not. R. Astron. Soc.* **1992**, *258*, 82–94. [[CrossRef](#)]
132. Magorrian, J.; Tremaine, S.; Richstone, D.; Bender, R.; Bower, G.; Dressler, A.; Faber, S.M.; Gebhardt, K.; Green, R.; Grillmair, C.; et al. The Demography of Massive Dark Objects in Galaxy Centers. *Astron. J.* **1998**, *115*, 2285–2305. [[CrossRef](#)]
133. Läscher, R.; Ferrarese, L.; van de Ven, G. Supermassive Black Holes and Their Host Galaxies. I. Bulge Luminosities from Dedicated Near-infrared Data. *Astrophys. J.* **2014**, *780*, 69. [[CrossRef](#)]
134. Ferrarese, L.; Merritt, D. A Fundamental Relation between Supermassive Black Holes and Their Host Galaxies. *Astrophys. J. Lett.* **2000**, *539*, L9–L12. [[CrossRef](#)]
135. Gebhardt, K.; Bender, R.; Bower, G.; Dressler, A.; Faber, S.M.; Filippenko, A.V.; Green, R.; Grillmair, C.; Ho, L.C.; Kormendy, J.; et al. A Relationship between Nuclear Black Hole Mass and Galaxy Velocity Dispersion. *Astrophys. J. Lett.* **2000**, *539*, L13–L16. [[CrossRef](#)]
136. Gültekin, K.; Richstone, D.O.; Gebhardt, K.; Lauer, T.R.; Tremaine, S.; Aller, M.C.; Bender, R.; Dressler, A.; Faber, S.M.; Filippenko, A.V.; et al. The M- σ and M-L Relations in Galactic Bulges, and Determinations of Their Intrinsic Scatter. *Astrophys. J.* **2009**, *698*, 198–221. [[CrossRef](#)]
137. McConnell, N.J.; Ma, C.P. Revisiting the Scaling Relations of Black Hole Masses and Host Galaxy Properties. *Astrophys. J.* **2013**, *764*, 184. [[CrossRef](#)]
138. van den Bosch, R.C.E. Unification of the fundamental plane and Super Massive Black Hole Masses. *Astrophys. J.* **2016**, *831*, 134. [[CrossRef](#)]
139. Cappellari, M.; Verolme, E.K.; van der Marel, R.P.; Verdoes Kleijn, G.A.; Illingworth, G.D.; Franx, M.; Carollo, C.M.; de Zeeuw, P.T. The Counterrotating Core and the Black Hole Mass of IC 1459. *Astrophys. J.* **2002**, *578*, 787–805. [[CrossRef](#)]
140. Krajnović, D.; McDermid, R.M.; Cappellari, M.; Davies, R.L. Determination of masses of the central black holes in NGC 524 and 2549 using laser guide star adaptive optics. *Mon. Not. R. Astron. Soc.* **2009**, *399*, 1839–1857. [[CrossRef](#)]
141. Ferrarese, L.; Ford, H.C.; Jaffe, W. Evidence for a Massive Black Hole in the Active Galaxy NGC 4261 from Hubble Space Telescope Images and Spectra. *Astrophys. J.* **1996**, *470*, 444. [[CrossRef](#)]
142. Sarzi, M.; Rix, H.W.; Shields, J.C.; Rudnick, G.; Ho, L.C.; McIntosh, D.H.; Filippenko, A.V.; Sargent, W.L.W. Supermassive Black Holes in Bulges. *Astrophys. J.* **2001**, *550*, 65–74. [[CrossRef](#)]
143. Dalla Bontà, E.; Ferrarese, L.; Corsini, E.M.; Miralda-Escudé, J.; Coccato, L.; Sarzi, M.; Pizzella, A.; Beifiori, A. The High-Mass End of the Black Hole Mass Function: Mass Estimates in Brightest Cluster Galaxies. *Astrophys. J.* **2009**, *690*, 537–559. [[CrossRef](#)]
144. Walsh, J.L.; Barth, A.J.; Ho, L.C.; Sarzi, M. The M87 Black Hole Mass from Gas-dynamical Models of Space Telescope Imaging Spectrograph Observations. *Astrophys. J.* **2013**, *770*, 86. [[CrossRef](#)]
145. Miyoshi, M.; Moran, J.; Herrnstein, J.; Greenhill, L.; Nakai, N.; Diamond, P.; Inoue, M. Evidence for a black hole from high rotation velocities in a sub-parsec region of NGC4258. *Nature* **1995**, *373*, 127–129. [[CrossRef](#)]
146. Greene, J.E.; Peng, C.Y.; Kim, M.; Kuo, C.Y.; Braatz, J.A.; Impellizzeri, C.M.V.; Condon, J.J.; Lo, K.Y.; Henkel, C.; Reid, M.J. Precise Black Hole Masses from Megamaser Disks: Black Hole-Bulge Relations at Low Mass. *Astrophys. J.* **2010**, *721*, 26–45. [[CrossRef](#)]
147. Kuo, C.Y.; Braatz, J.A.; Condon, J.J.; Impellizzeri, C.M.V.; Lo, K.Y.; Zaw, I.; Schenker, M.; Henkel, C.; Reid, M.J.; Greene, J.E. The Megamaser Cosmology Project. III. Accurate Masses of Seven Supermassive Black Holes in Active Galaxies with Circumnuclear Megamaser Disks. *Astrophys. J.* **2011**, *727*, 20. [[CrossRef](#)]
148. Davis, T.A.; Bureau, M.; Cappellari, M.; Sarzi, M.; Blitz, L. A black-hole mass measurement from molecular gas kinematics in NGC4526. *Nature* **2013**, *494*, 328–330. [[CrossRef](#)]
149. Barth, A.J.; Boizelle, B.D.; Darling, J.; Baker, A.J.; Buote, D.A.; Ho, L.C.; Walsh, J.L. Measurement of the Black Hole Mass in NGC 1332 from ALMA Observations at 0.044 arcsecond Resolution. *Astrophys. J. Lett.* **2016**, *822*, L28. [[CrossRef](#)]
150. Onishi, K.; Iguchi, S.; Davis, T.A.; Bureau, M.; Cappellari, M.; Sarzi, M.; Blitz, L. WISDOM project—I. Black hole mass measurement using molecular gas kinematics in NGC 3665. *Mon. Not. R. Astron. Soc.* **2017**, *468*, 4663–4674. [[CrossRef](#)]

151. Smith, M.D.; Bureau, M.; Davis, T.A.; Cappellari, M.; Liu, L.; Onishi, K.; Iguchi, S.; North, E.V.; Sarzi, M.; Williams, T.G. WISDOM project—VII. Molecular gas measurement of the supermassive black hole mass in the elliptical galaxy NGC 7052. *Mon. Not. R. Astron. Soc.* **2021**, *503*, 5984–5996. [[CrossRef](#)]
152. Cohn, J.H.; Walsh, J.L.; Boizelle, B.D.; Barth, A.J.; Gebhardt, K.; Gültekin, K.; Yıldırım, A.; Buote, D.A.; Darling, J.; Baker, A.J.; et al. An ALMA Gas-dynamical Mass Measurement of the Supermassive Black Hole in the Local Compact Galaxy UGC 2698. *Astrophys. J.* **2021**, *919*, 77. [[CrossRef](#)]
153. Zhang, H.; Bureau, M.; Smith, M.D.; Cappellari, M.; Davis, T.A.; Dominiak, P.; Elford, J.S.; Liang, F.H.; Ruffa, I.; Williams, T.G. WISDOM Project—XIX. Figures of merit for supermassive black hole mass measurements using molecular gas and/or megamaser kinematics. *Mon. Not. R. Astron. Soc.* **2024**, *530*, 3240–3251. [[CrossRef](#)]
154. Onishi, K.; Iguchi, S.; Sheth, K.; Kohno, K. A Measurement of the Black Hole Mass in NGC 1097 Using ALMA. *Astrophys. J.* **2015**, *806*, 39. [[CrossRef](#)]
155. van den Bosch, R.C.E.; Gebhardt, K.; Gültekin, K.; van de Ven, G.; van der Wel, A.; Walsh, J.L. An over-massive black hole in the compact lenticular galaxy NGC 1277. *Nature* **2012**, *491*, 729–731. [[CrossRef](#)] [[PubMed](#)]
156. Oosterloo, T.; Morganti, R.; Crocker, A.; Jütte, E.; Cappellari, M.; de Zeeuw, T.; Krajnović, D.; McDermid, R.; Kuntschner, H.; Sarzi, M.; et al. Early-type galaxies in different environments: An HI view. *Mon. Not. R. Astron. Soc.* **2010**, *409*, 500–514. [[CrossRef](#)]
157. Serra, P.; Oosterloo, T.; Morganti, R.; Alatalo, K.; Blitz, L.; Bois, M.; Bournaud, F.; Bureau, M.; Cappellari, M.; Crocker, A.F.; et al. The ATLAS^{3D} project—XIII. Mass and morphology of H I in early-type galaxies as a function of environment. *Mon. Not. R. Astron. Soc.* **2012**, *422*, 1835–1862. [[CrossRef](#)]
158. Maccagni, F.M.; Serra, P.; Gaspari, M.; Kleiner, D.; Morokuma-Matsui, K.; Oosterloo, T.A.; Onodera, M.; Kamphuis, P.; Loi, F.; Thorat, K.; et al. AGN feeding and feedback in Fornax A. Kinematical analysis of the multi-phase ISM. *Astron. Astrophys.* **2021**, *656*, A45. [[CrossRef](#)]

Disclaimer/Publisher’s Note: The statements, opinions and data contained in all publications are solely those of the individual author(s) and contributor(s) and not of MDPI and/or the editor(s). MDPI and/or the editor(s) disclaim responsibility for any injury to people or property resulting from any ideas, methods, instructions or products referred to in the content.